Carbon Nanostructures for Use in Oxygen Reduction

Honors Thesis for Graduation with Distinction

Submitted May 2010

By Douglas S Knapke

The Ohio State University

Department of Chemical and Biomolecular Engineering

140 West 19th Avenue

Columbus, OH 43210

Honors Committee:

Professor Umit S. Ozkan, Advisor

Professor James Rathman

I. Acknowledgements

Without the help of several important individuals this thesis would not have been possible. I would like to acknowledge them for their help and support. First and foremost, I would like to thank my mentor, Elizabeth Biddinger. Without her direction, dedication and technical knowledge I would not have been able to perform research or complete this thesis. I have worked with Elizabeth for three years and she has been endlessly patient and more than willing to help me develop as a researcher and as an individual. I would also like to thank Dr. Umit Ozkan. Through her hard work and dedication to her students she has provided the guidance and framework for me and others to thrive and reach our full potential. I can honestly say she is one of the kindest, most sincere individuals I have ever had the chance to meet. Next, I want to thank the other Heterogeneous Catalysis Research Group members, especially PEM team, for helping me to resolve issues as they arose and for making my time in the laboratory a fun, enjoyable experience. I would like to thank my family. Without their support and value system, I would have long ago given up on research and chemical engineering in general. Finally, I would like to thank my fiancée, Megan Gariety, who has supported me through the stress of completing this thesis while finishing my degree.

II. Abstract

The Proton Exchange Membrane Fuel Cell (PEMFC) has shown promise as a replacement to the current media of transportation, the Internal Combustion Engine (ICE). Proliferation of this technology has been hampered by the cost and performance issues associated with the current cathodic, oxygen reduction reaction (ORR) catalyst, platinum. It has been shown that nitrogen – containing carbon nanofibers (N-CNFs) formed by the chemical vapor deposition (CVD) of hydrocarbons onto metal catalysts have activity for ORR. Despite being less expensive than platinum, N-CNFs still lack the performance of conventional catalysts. Understanding and controlling the growth of these nanofibers will allow researchers to engineer N-CNFs with optimum catalytic properties for ORR. For this reason, two studies were completed to better understand the CVD of hydrocarbon carrier gases over metallic catalysts. The first studied the effect of thiophene (C_4H_4S) addition to the acetonitrile (CH_3CN) pyrolysis over a 2% Fe/ MgO growth catalyst at 900°C. The samples were characterized by Transmission Electron Microscopy (TEM), Temperature Programmed Oxidation (TPO) Experiments, Rotating Ring-Disk Electrode (RRDE) half cell testing, and nitrogen physisorption. It was found that addition of thiophene to the reactant acetonitrile causes an increase in carbon deposition onto the metallic growth catalyst. Increased growth caused an accompanying change in morphology from pristine stacked-cups to a more disordered stacked cup conformation. Despite a morphological shift, ORR activity and selectivity was not significantly affected as compared to the catalysts grown with acetonitrile only. In another study, the deposition of CO/H_2 (4:1) over 6:4, 7:3 and 8:2 Fe:Cu co-precipitation catalysts were studied at temperatures ranging from 625°C-725°C and the nanofibers evaluated. The samples produced were characterized by TEM, Raman spectroscopy, and hydrophobicity testing. Samples showed remarkable growth, depositing up to 14 times the mass of the Fe: Cu growth catalysts. CVD at 725°C showed a

decrease in growth and an increase in encapsulation of the metal particle suggesting partial deactivation of the growth catalyst. TEM characterization of the nanofibers showed that most of the catalyst formulations resulted in a platelet morphology, but other less-structured fiber types were observed. At high temperatures CVD favored the formation of multi-walled nanotubes (MWNTs). Analyses of Raman spectra reveal the presence of oxygen functionalities on the surface of the catalysts. In addition, it showed that the CNF have a large amount of graphitic edge plane exposure, indicating that they can be functionalized with nitrogen for use in ORR.

III. Table of Contents

List of Figures

List of Tables

IV. Introduction

A. Motivation

The finite supply of crude oil and the effect of increased atmospheric carbon dioxide (CO_2) have called into question the economic and environmental sustainability of the current internal combustion engine (ICE) driven model for transportation[1]. While world crude oil reserves are virtually unknowable [2] , it is clear that the quality and ease of extraction of crude oil are both declining as higher quality crudes become depleted. This fact compounded with the imminent increase in oil demand from the rapidly industrializing, high population BRIC (Brazil, Russia, India, China) countries [3]call into question the long-term economic viability of using gasoline as the primary fuel for transport. Because of this, scientists have proposed several alternative models for future transportation including one centered on hydrogen and the Proton Exchange Membrane fuel cell (PEMFC). The PEMFC uses hydrogen and oxygen as fuel to produce the more thermodynamically stable water, which liberates energy. PEMFCs offer several advantages over ICEs including higher theoretical efficiency, no moving parts, low noise, and minimal emissions. In addition, PEMFCs are compact and operate at a low temperatures (60 – 80 °C), which allows for fast start-up and low thermal stress on components. Despite these advantages, PEM fuel cells have several technological limitations that must be overcome before the technology can be commercially viable.

B. Fuel Cell Catalysis

A schematic of a hydrogen fuel cell can be seen in Figure IV-1, below.

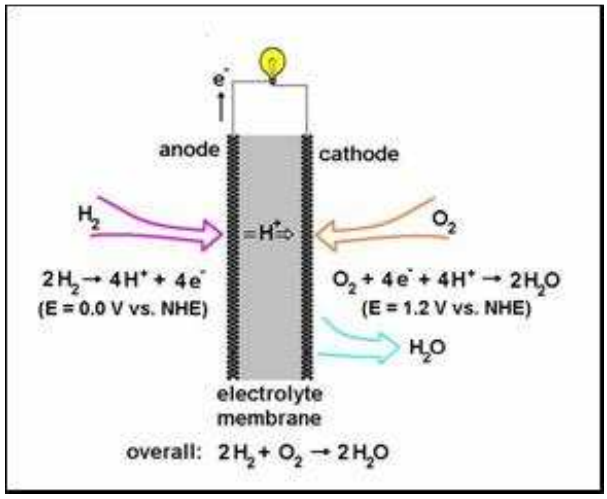

Figure IV-1: PEM Fuel Cell Schematic.

DRAWING BY PAUL MATTER

The PEM fuel cell operates on two half reactions; the anodic reaction, shown on the left side of the figure, ionizes hydrogen into protons (H^+) and elections (e^-) via the following half reaction[4].

$$2H_2 \rightarrow 4H^+ + 4e^- \qquad E° = 0.0\ V\ vs. NHE \qquad (equation\ IV.1)$$

The protons travel across a polymer electrolyte membrane (most commonly sulfonated polytetrafluoroethylene)) that is selectively permeable to the H^+ ions. The electrons move through an external circuit and perform useful work. At the cathode, the protons and electrons recombine with oxygen to form water in the oxygen reduction reaction (ORR).

$$O_2 + 4e^- + 4H^+ \rightarrow 2H_2O \qquad E° = 1.229\ V\ vs\ NHE \qquad (equation\ IV.2)$$

Alternatively, the hydrogen and oxygen can combine to form hydrogen peroxide (H_2O_2).

$$O_2 + 2e^- + 2H^+ \rightarrow H_2O_2 \qquad E° = 0.695\,V\ vs\ NHE \qquad (equation\ IV.3)$$

Hydrogen peroxide will corrode the fuel cell, reducing its lifetime considerably[5]. Selectivity is a measure of the ratio of water to hydrogen peroxide produced and is another measure of ORR catalyst effectiveness.

The two desired half reactions (Equations IV.2-3) are conventionally catalyzed by platinum, but the cathodic reaction (ORR) is kinetically limited (Equation IV.2). Because of this, the cathode causes severe efficiency degradations and requires higher platinum loadings[6]. These high loadings and efficiency losses are two of the main barriers to the economic viability of PEM fuel cells. For instance, in an 85 KW fuel cell system capable of performance similar to a 100 HP engine, it is estimated that platinum costs alone would be $3200-$4500 dollars using March 2010 market prices [7-9].

Extensive research has been conducted to improve the performance and/or decrease the cost of the cathodic ORR catalysts through the use of alternative non-noble metal, carbon based catalysts. The first of these catalysts, first synthesized in the 1960s, were FeN_4 or CoN_4 macrocycles adsorbed on a carbonaceous support and were designed to mimic oxygen affixation properties of the hemoglobin active site[10, 11]. These catalysts were found to quickly break down in a fuel cell environment. Later, it was shown that heat treatment in an inert environment improved the stability and activity of these catalysts[12]. Despite their promise, these marcocycles were difficult and expensive to produce and offered few economic advantages over conventional platinum. Since then it has been shown by the several groups, that pyrolysis of a variety of non-macrocycle metal precursors in the presence of nitrogen and carbon results in active ORR catalysts[13-15]. The Heterogeneous Catalysis Research Group (HCRG) at Ohio State, have shown that nitrogen-containing carbon nanofibers (N-CNFs) have substantial ORR catalytic activity [16-20]. N-CNFs are composed primarily of nanostructured graphitic carbon with nitrogen dispersed through the graphitic matrix[18]. They can be made by functionalizing

existing carbon structures with ammonia [21, 22] or by pyrolysis of a nitrogen containing molecule [23, 24]. While less expensive, current ORR carbon-nitrogen catalysts are still less active than platinum catalysts for ORR. The amount of ORR activity and selectivity in these catalysts is influenced by a number of factors including nanofiber structure, amount of pyridinic nitrogen, and the presence of oxygen functionalities in the matrix of the fiber [17, 25]. If nanofiber synthesis could be understood and controlled it would be possible to design an N-CNF with optimum structural characteristics for ORR catalysis.

Depending on reaction conditions, carrier gas, and growth catalyst, N-CNFs with different length, diameter, and graphitic orientation can be synthesized[26]. Figure IV-2 below shows a number of commonly observed CNF and N-CNF nanostructures.

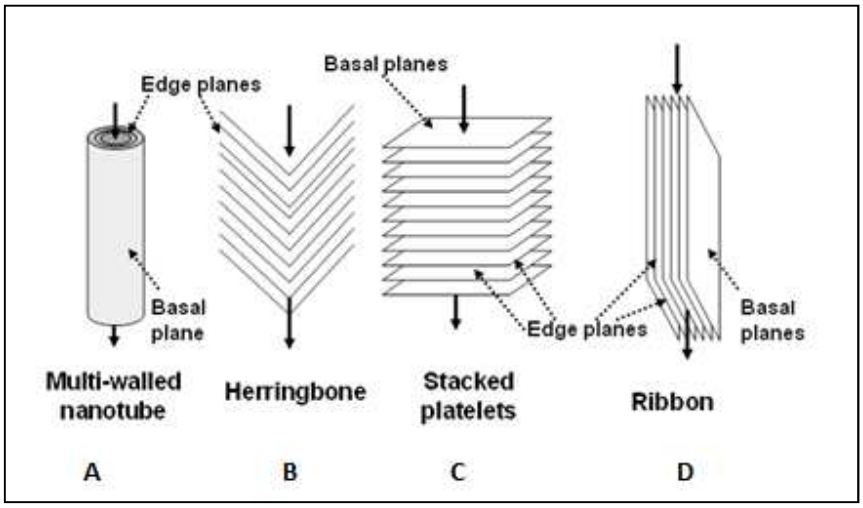

Figure IV-2: Common Nanofiber Morphologies

Drawing By Elizabeth Biddinger

Figure IV-2 (B) and Figure IV-2 (C) show herringbone and stacked platelet type nanofibers. These nanofibers consist of graphene sheets with edges perpendicular (stacked platelets) or at a shallow angle (herringbone) to the longitudinal axis and have high edge plane exposure. Several workers have concluded that the effectiveness of carbon-based ORR catalysts is linked to amount of edge plane

exposure present in the N-CNF. Literature suggests that the active site in these catalysts in probably either pyridinic nitrogen[17] or Fe coordinated nitrogen carbon sites [27], located in micropores on the graphite edge planes of the fiber. The edge plane exposure has been observed to increase the hydrophilicity [25] and ORR activity of these molecules. Because there is little continuity along the basal plane, samples containing a large amount of these nanostructures are much less conductive than highly-oriented polycrystalline graphite (HOPG) [28]. Multi-walled nanotubes (MWNTs) are depicted in Figure IV-2 (A). A multi-walled nanotube consists of graphene sheets rolled around a vertical axis. In contrast to the previous nanostructures discussed, the high basal plane-to-edge-plane ratio results in lower reactivity and hydrophilicity, and high conductivity.

An optimum ORR catalyst would be highly conductive for efficient electron transfer through the fuel cell, hydrophilic for effective water management, and have high active site density. This would require a fiber with high edge plane exposure and continuity along the basal plane. Figure IV-2(D) shows a ribbon nanofiber. This nanostructure has both high edge plane exposure and continuity along the growth axis. Unfortunately, this type of fiber has, to date, not been incorporated with nitrogen and tested for ORR activity in our laboratory due to inability to form the nanofiber at high purity.

C. Carbon-Nitrogen Catalyst Growth

Nitrogen containing carbon nanofibers (N-CNFs) have been synthesized using several techniques. Nitrogen can be directly incorporated by pyrolysis with nitrogen containing molecule, such as acetonitrile (CH_3CN) over a transition metal on a high surface area support such as 2% Fe/MgO at high temperature. The HCRG research group has been particularly active in studying this formulation. They have shown that preparation in this manner generally results in stacked cup N-CNF nanostructures

similar those shown in Figure IV-3 below. These nanofibers have 4-10% nitrogen incorporation and have relatively good catalytic behavior but are still not as active as platinum[19].

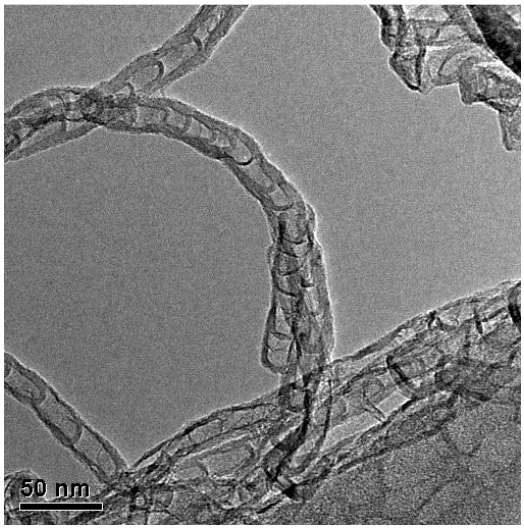

Figure IV-3: N-CNFs Formed by the Pyrolysis of CH_3CN over 2% Fe/MgO

Alternatively, carbon nanofibers with edge plane exposure can be post-treated in ammonia atmosphere to make N-CNFs [29]. CNFs have been observed to grow over a variety of catalysts under a multitude of growth conditions [30]. For instance, CO/H_2 reactant gases have been shown to deposit large amounts of nanostructured carbon over metallic catalysts at temperatures below 800°C [31-33]. This two-step method is advantageous because it allows the ORR catalyst researcher to investigate a wider array of growth variables to design a catalyst with a specific structure. In addition, nitrogen incorporation can be better controlled through variation in post-treatment conditions[34]. Because there are so many growth variables, research must be done to determine how each variable affects the growth and morphology of the carbon fiber.

D. Experimental Objectives

Broadly stated, the purpose of this thesis is to study the effect of varied synthesis conditions on the final morphology of CNFs and N-CNFs. Specifically, this involves the testing of two hypotheses. The first study attempts to determine the structural dependence of carbon nanofibers on growth catalyst composition and pyrolysis temperature. This was done by studying the CNFs produced by the pyrolysis of CO/H_2 over bimetallic iron/copper catalysts. This formulation has been reportedly used to produce ribbon nanofibers[31], which would be a desirable ORR catalyst nanostructure. The fibers were later characterized by TEM, Raman spectroscopy, and hydrophobicity testing.

The second set of experiments is aimed at proving (1) whether thiophene (C_4H_4S) introduction to acetonitrile pyrolysis can enhance the growth of N-CNFs as has been reported for non-nitrogen containing CNFs[35-37] and (2) determine the morphological and ORR catalytic consequences of such an addition. In order to do this, a carrier gas was bubbled through a mixture of acetonitrile and varying levels of thiophene. The mass of carbon deposited was recorded and the samples were characterized by using nitrogen physisorption, TEM, Temperature Programmed Oxidation (TPO) and hydrophobicity testing. Catalytic behavior in oxygen reduction was characterized using a rotating ring disk electrode (RRDE) half cell technique.

V. Literature Review

A. Growth Mechanism

The growth mechanism by which carbon in the vapor phase is deposited to form carbon nanofibers (CNFs) at high temperatures has been studied extensively by a number of researchers [38-43]. The catalytic nature of this process was first documented by Tesner and coworkers who were the first to associate filamentous carbon growth with metal particles[44]. Since then, several interesting in-situ electron microscopy studies have been conducted to directly observe carbon nanofiber growth on a metal substrate. In one such study, Baker *et al.* studied the decomposition of acetylene over small metal particles at elevated temperatures[38]. Frame by frame analysis of this experiment resulted in the proposal of the following growth mechanism: (1) the absorption and dissociation of the reactant hydrocarbon on the surface of the metal particle (2) the diffusion of the reactant through the metal particle and (3) deposition of the carbon atoms on the opposite side of the metal particle. The rate determining step in this process is thought to be the diffusion of the gas through the metal particle[39]. This proposed mechanism was evaluated by studies performed by Helveg *et al*[45]. Helveg was able to further characterize the nature of carbon growth by studying the deposition of methane onto supported nickel catalysts at 500°C through in-situ electron microscopy imaging. It was found that carbon nanofibers were developed through reaction-induced reshaping of the nickel catalyst that involved oscillations between spherical and elongated shapes. Repetitive formation of monotonic edge steps on the nickel surface was found to facilitate nucleation of graphene sheets on the opposite side of the particle. In addition, the authors proposed a mechanism, supported by density functional theory calculations that the catalyst particle was diffusing *across* the surface of the particle rather than through it.

A wide variety of catalysts, reactant gases and temperatures have been shown to produce different types of filamentous carbon. Indeed, pyrolysis of methane, carbon monoxide, synthesis gas (CO/H_2), acetylene, and ethane over alloys of iron, cobalt, nickel, chromium, vanadium, copper and molybdenum and have all yielded different types of carbon deposits[30]. Minute differences in catalyst composition and shape, reaction temperature, and reactant gas all have an effect on the overall size and morphology of the carbon nanofibers [46]. In particular, $CO:H_2$ systems have been shown to produce carbon nanofibers readily over supported and unsupported iron based catalysts through the disproportionation of CO via the Boudouard reaction[33, 47, 48]:

$$2CO \rightarrow C + CO_2 \qquad Equation\ VI.1$$

This reaction is known to favor carbon formation at temperatures below 700°C [46, 49].

It has been reported that addition of hydrogen to the CO reactant gas greatly enhances CNF growth in this system. The reasons for this are twofold. (1) the occurrence of a secondary reaction (Equation VI.2) to produce solid carbon can occur and (2) hydrogen adsorbed on the catalyst surface is thought to catalyze the Boudouard reaction[47].

$$CO + H_2 \rightarrow C + H_2O \qquad Equation\ VI.2$$

Dry et al. suggest that chemisorbed hydrogen induces electron donation to the iron surface. This electron enrichment increases the Fe-CO bond strength which in turn weakens the C-O bond[50]. The C-O bond is more easily severed to produce pure carbon materials such as carbon nanofibers. Study of the pyrolysis reaction effluent gases indicate that 4:1 CO-H_2 mixtures over Fe catalysts yield high amounts of solid carbon while minimizing the production of methane via CO methanation, as shown in the following reaction[47]:

$$CO + 3H_2 \rightarrow CH_4 + H_2O \qquad Equation\ VI.3$$

Production of CH_4 is undesired because it can cause further undesired side reactions and create non-homogenous mixtures of CNFs.

B. Observed CNF Growth of CO: H2 over Metallic Catalysts

The choice of transition metal catalyst and reaction temperature has been varied for formulations of CO:H_2 and the effects studied by several researchers. The results of several studies of CO/H_2 and C_2H_4/ H_2 growth over various reaction conditions has been compiled in Table IV.1 below.

Table V-1 : Observed Catalyst Morphologies at Different Temperatures

Gas (ratio)	Catalyst (ratio)	Temperature (°C)	Duration (h)	Morphology	Reference
CO/H_2 (4:1)	Fe	600	1.5	Stacked Platelets	[48]
CO/H_2 (4:1)	Fe / SiO_2	600	1.5	Herringbone	[48]
C_2H_4 / H_2 (4:1)	Fe: Cu (7:3)	600	1.5	Tubular	[48]

CO/H_2 (4:1)	Fe	600	1.5	Platelet	[47]
CO/H_2 (4:1)	Fe/Ni (9:1)	600	1.5	Herringbone	[47]
CO/H_2	Fe/Ni (1:3)	600	1.5	Tubular	[47]
C_2H_4/H_2 (4:1)	Fe:Cu (9:1)	600	2	Tubular	[51]
C_2H_4/H_2 (4:1)	Fe: Cu (7:3)	600	2	Herringbone	[51]
$CO/C_2H_4/H_2$ (3:1:1)	Fe: Cu (7:3)	600	3	Platelet	[46]
$CO/C_2H_4/H_2$ (1:1:3)	Fe: Cu (7:3)	600	3	Herringbone	[46]
$CO/C_2H_4/H_2$ (1:3:1)	Fe: Cu (7:3)	600	3	Spiral	[46]
CO/H_2 (4:1)	Fe: Cu (7:3)	600	2	Platelet	[33]
$CO:H_2$ CO/H2 (1:4)	Fe: Cu (7:3)	600	2	Herringbone	[33]
CO/H_2 (4:1)	Fe: Cu (1:9)	600	2	Amorphous	[33]
CO/H_2 (4:1)	Fe: Cu (7:3)	700	2	Tubular	[33]

Rodriguez and coworkers[48] reported that the pyrolysis of $CO:H_2$ (4:1) at 600°C over unsupported Fe catalyst yielded stacked platelet structures while Fe catalysts supported over silica (SiO_2) yielded fibers with graphene sheets aligned parallel to the growth axis. It was observed that nanofibers grown from unsupported fibers have much higher variability in width. In addition, the authors note that interaction of the gas molecule with the catalyst particle can result in a process known as surface reconstruction where chemisorbed gas induces mobility of the surface atoms of the solid to well-defined crystallographic orientations. These orientations in turn determine the final morphology of the particle.

Variation in temperature has been known to dramatically influence final CNF structure. In a study by Park and co-workers, the influence of temperature and catalyst composition were studied in an 4:6 Fe:Ni catalyst system[49]. It was observed that the pyrolysis of $CO:H_2$ (4:1) at 550°C-600°C yielded

platelet-type CNFs. The increase of pyrolysis temperature to 650°C resulted in a shift to nanofibers with a graphitic orientation largely parallel to the growth axis (MWNTs). Finally, at temperatures above 650°C the catalyst became encapsulated in a graphitic shell and catalyst yields decline markedly.

Copper addition to electron rich transition metals, such as iron and nickel, has been shown to influence CNF growth. Interactions between "electron-rich" and "electron-poor" constituents can cause large perturbations on the surface of the growth catalyst which, in turn, change the catalytic properties of the particle[52]. In broad study of Fe:Cu catalysts, bimetallics with compositions of 9:1, 7:3, 5:5, 3:7 and 1:9 Fe:Cu were synthesized and CNFs grown at temperatures between 500°C-700°C with C_2H_4/H_2 and CO/H_2 reactant gases[33]. Temperature Programmed Oxidations (TPOs) of the CO/H_2 (4:1) CNFs showed that those grown with lower ratios of Fe:Cu oxidized at lower temperatures indicating less graphitic structures.

Variation in temperature was also studied. An X-ray diffraction study showed that samples grown at higher temperatures had a more graphitic structure. TEM images of 7:3 Fe:Cu growth at 600°C and 700°C were presented. The higher temperature sample showed vertical alignment of the carbon nanofibers whereas the lower temperature samples showed a platelet structure.

In a patent filed by Baker[31], a corresponding author to the papers discussed above, it is noted that ribbon nanofibers are formed by the deposition of $CO:H_2$ over Fe:Cu catalyst somewhere between 625°C and 725°C. As discussed previously, these nanostructures are of great interest to ORR catalysis because of their proposed high conductivity and functionalization potential.

C. Sulfur Growth Promotion

Several researchers have reported that sulfur addition to the hydrocarbon reactant stream and subsequent chemisorption onto metal surface enhances the growth of CNFs[53, 54]. Pretreatment of metal particles with H_2S, direct introduction of H_2S to the reactant stream, and addition of thiophene have all been used to successfully promote carbon deposition [35, 36, 55] . For instance in a study done by Kim and coworkers[35], it was reported that pretreatment of a cobalt growth catalyst with 17 ppm H_2S increased carbon deposition from 4.5% to 70% in a C_2H_4/H_2 system. Treatment at higher and lower concentrations of H_2S resulted in a decrease in growth; this indicates that there exists an optimal concentration of sulfur on the surface of the metal particle. Temperature Programmed Oxidations (TPOs) of the samples showed that increased growth was accompanied by a decrease in graphitization. Evidence of sulfur induced morphological shifts was also observed by other researchers [54, 56]. Fan *et al.* [57] found in his study of pilot scale production of CNFs, that by varying that concentration of thiophene in the ferrocene catalyst gas, CNF width could be controlled.

Two mechanisms have been proposed to explain the sulfur growth promotion of CNFs. Kim and coworkers contend that electronic changes induced by the adherence of sulfur to the metal surface are responsible for the changes in growth[35]. They argue that at low coverage, the strongly bound sulfur facilitates reconstruction of the surface layers, a step which may favor carbon-carbon bond rupture in the reactant hydrocarbon. This produces species that diffuse through the particle and precipitate on the rear face of the metal. At higher concentrations, the metal particle is completely covered by sulfur and growth diminishes. This explains why growth decreases after optimal sulfur addition. Alternatively, Tibbetts [58] and coworkers hypothesize that sulfur-induced growth promotion can be explained by a reduction of melting point in the metal sulfide. The reduced melting point allows for a liquid or pseudo-liquid state that enhances the fiber nucleation by a vapor-liquid-solid process. A higher than optimum

concentration of sulfur will move the metal away from the eutectic point thus explaining the presence of a growth maximum. Until this study, no publications were found that studied the effect of sulfur addition to acetonitrile pyrolysis.

VI. Experimental Methods

A. Materials Preparation

Nitrogen-containing Carbon Nanofibers (N-CNFs)

2 wt % Fe / MgO was used as a growth catalyst in the preparation of nitrogen containing carbon nanofibers (N-CNFs). It was prepared using incipient wetness impregnation technique (IWI). The IWI technique is designed to saturate the micropores of the support (MgO) with growth catalyst (2 wt % Fe). This was done by, first, determining the mircoporous volume of the support by BET surface area analysis. An Iron acetate ($Fe(C_2H_3O_2)_2$)/ deionized water solution was then prepared equal to the microporous volume at a concentration required to give 2 weight % Iron (Fe). The solution was deposited dropwise onto the catalyst and dried at 110°C for 1 day to drive off excess water. The iron acetate and high surface area magnesia precursors used for this study were purchased from Sigma – Aldrich.

Acetonitrile (CH_3CN, Fisher, Optima grade) –Thiophene ((C_4H_4S, Acros Organics) pyrolysis was performed by placement of 2 grams 2%Fe/MgO in a high temperature furnace. Temperature was increased 10°C / min to 900°C in an inert atmosphere. 150 mL/ min of nitrogen was then bubbled through an Acetonitrile/Thiophene solution and introduced to the furnace for 2 hours. The sample was cooled under a nitrogen atmosphere to room temperature and the amount of carbon deposition measured.

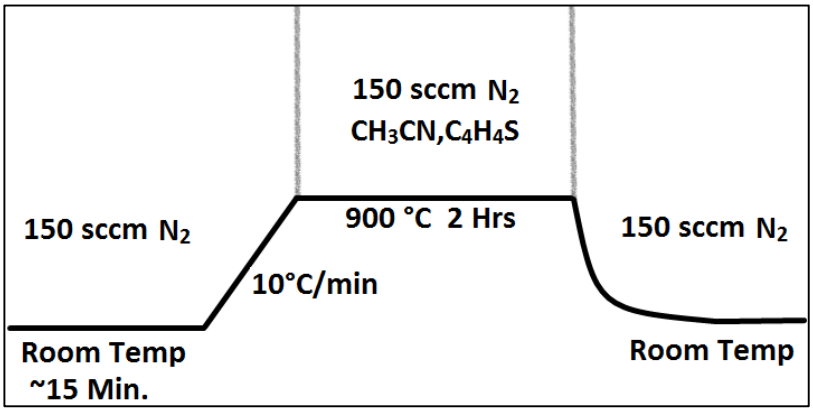

Figure VI-1: Experimental Conditions for Acetonitrile Pyrolysis

Thiophene was introduced to the acetonitrile bubbler at concentrations of 1.8, 3.6, 5.5, 7.3, 8.9, 11.5 mol%. In addition, samples were grown with pure acetonitrile and pure thiophene reactants. The sample weight was recorded before and after pyrolysis. Samples were then washed in 2.4 M hydrochloric acid (HCl) at 60°C, vacuum filtered and rinsed with deionized water to remove exposed metal particles; samples were allowed to dry at 110°C for 1 day.

Carbon Nanofiber Preparation

Carbon nanofibers were synthesized by chemical vapor deposition (CVD) of 4:1 carbon monoxide (CO) / hydrogen (H_2) over bimetallic iron-copper growth catalysts. Growth catalysts were prepared by co-precipitation of Iron (III) nitrate ($Fe(NO_3)_3$) and Cu(II) nitrate ($Cu(NO_3)_2$) with ammonium carbonate ($(NH_4)_2CO_3$)) in 6:4, 7:3, and 8:2 Fe:Cu molar ratios in order to study the effect of catalyst composition on fiber morphology. The bimetallic catalysts were then dried at 110°C overnight to drive off water and crushed to a fine powder with a pestle and mortar. 100 mg of catalyst was placed a quartz boat in the catalyst furnace where the temperature was increased at 10°C/min to 600°C. The catalyst was reduced for 14.5 hours in a 5% H_2/He atmosphere. After flushing with helium for ½ hour,

the temperature was then increased at 10°C/min to the final growth temperature and the $CO:H_2$ reactant stream was introduced. Fibers were grown at 625°C, 650°C, 675°C, and 725°C for 2 hours. A total of 12 samples were synthesized, one at each temperature/catalyst ratio combination. For the sake of brevity, samples will be referred to by their specific growth combination. For instance, the CNFs deposited over a 7:3 Fe:Cu catalyst at 650°C are labeled CNF[7:3, 650°C]. After growth, each sample was washed in 1 M HCl at 60°C, vacuum filtered and rinsed with deionized water to remove any exposed metallic particles. The samples were allowed to dry at 110°C for 1 day.

B. Characterization Techniques

Transmission Electron Microscopy (TEM)

Transmission electron microscopy was performed by my associate, Elizabeth Biddinger, in order to characterize the morphology of the nanofibers synthesized. A FEI Tecnai F20 XT Transmission Electron Microscope operated at 200 kV was used to examine samples suspended in ethanol and applied to a lacey-formvar carbon supported on a 200 mesh copper TEM grid.

Nitrogen Physisorption

BET (Brunauer, Emmett, Teller) surface area and BJH (Barret-Joyner-Halenda) pore volume of catalysts was determined through nitrogen physisorption experiments performed using a Micromeritics ASAP 2010.

Electrochemical Characterization

ORR catalyst activity and selectivity testing was conducted using a model 636 Rotating Ring Disk Electrode (RRDE) half cell connected to PAR bi-stat. The RRDE setup is shown in Figure VI-2 below.

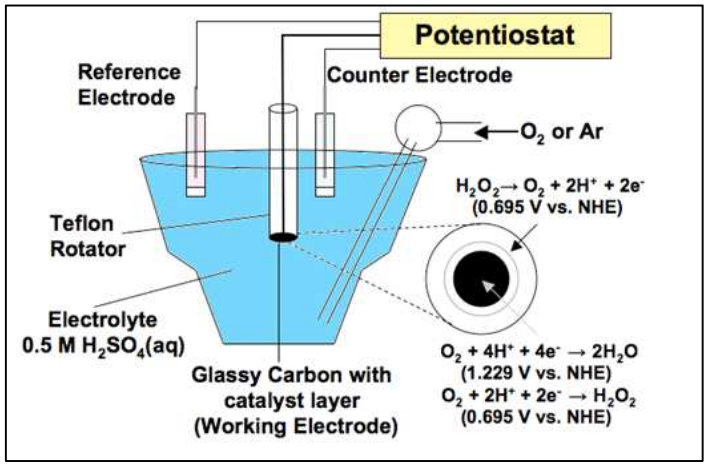

Figure VI-2: The RRDE Test Assembly

Figure by Dieter Von Deak

The RRDE assembly consists of a 0.1642 cm^2 glassy carbon disk encircled by a platinum ring which can be rotated at specific rates using an electric motor. After 30 minutes of sonication, catalyst inks consisting of 1:10:160 (by mass) catalyst: Nafion in aliphatic alcohols: ethanol were prepared and dispersed onto the glassy carbon disk in 3 x 5 μL aliquots resulting in a catalyst loading of 426 $\frac{\mu g}{cm^2}$. The RRDE assembly was then lowered into the electrolyte, a 0.5 M solution of H_2SO_4. This setup mimics the ORR half cell reaction shown in Equation IV.1. H^+ ions are present in the H_2SO_4, and oxygen is dissolved into solution. Overpotential can be measured by observing when electron transfer begins relative to the theoretical voltage of 1.2 vs. NHE. Hydrogen peroxide formed can be detected by holding the ring at 1.2 V vs. NHE through the reaction:

$$H_2O_2 \rightarrow O_2 + 2e^- + 2H^+ \qquad E° = -0.0695\, V\ vs.\ NHE \qquad (equation\ VI.1)$$

Selectivity is reported as n, the average number of electrons transfer per oxygen molecule reacted. This is calculated by comparing the ring current (I_R) to the disk current (I_d) using the following equation[4]:

$$n = \frac{4I_d}{I_d + \left(\frac{I_r}{N}\right)} \qquad (equation\ VI.2)$$

Where N= 0.22 is the collection efficiency of the disk reported by the manufacturer. All voltages in the setup are measured against an Ag/AgCl (sat KCl) reference electrode and a Pt counter electrode was used to complete the circuit.

The experiments were performed by, first, saturating the H_2SO_4 solution with O_2 and taking an initial sweep from 1.2 to 0.0 to 1.2 vs NHE to remove gaseous O_2 from the catalyst pores and allow them to fill with solution[16]. All CVs were run at between these potentials unless otherwise noted. Argon was bubbled through the solution for 30 minutes. Next, consecutive CVs were taken at 50 mV/sec while the ring was held at 1.2 V vs. NHE and current measured until scans were repeatable to ensure that all oxygen had been removed from the system. A background scan (10 mV/sec) in argon was taken at 100 rpm while holding the ring constant at 1.2V vs. NHE. The electrolyte was again saturated with oxygen and CVs were run at 10 mV/sec with rotation rates of 0, 100 and 1000 rpm. The potential at which the catalyst separates from the argon baseline is defined as the onset of activity and gives the relative ORR activity of the catalyst.

Raman Spectroscopy

Raman spectroscopy was performed using a Horiba Jobin Yvon LabRam 300 confocal instrument. Spectra were attained with a He-Ne laser (633 nm) at 298 K by taking the average of 30 scans at 5 second exposure times at 50x magnification.

Hydrophobicity Testing

The relative hydrophobicity of the samples was examined by suspending 1 mg of catalyst in 10mL of DI water. The samples were sonicated for 30 minutes and then visually examined and compared.

Temperature Programmed Oxidation (TPO) Experiments

Temperature programmed oxidation experiments were performed using a MKS Cirrus residual gas analyzer to monitor the composition and oxidation temperature of the N-CNF – thiophene catalysts. The temperature was ramped 5°C/min to 800°C while from 10% O_2/Ar while scanning mass signals 1 – 100.

VII. Results and Discussion – $CO:H_2$ Grown Carbon Nanofibers

A. Raman Spectroscopy - Peak Identification

Raman spectroscopy was performed on all 12 of the acid washed CNFs synthesized via the CVD of $CO:H_2$ (4:1) over bimetallic Fe:Cu catalysts. A representative first order Raman spectra of the carbon nanofibers can be seen in Figure VII-1.

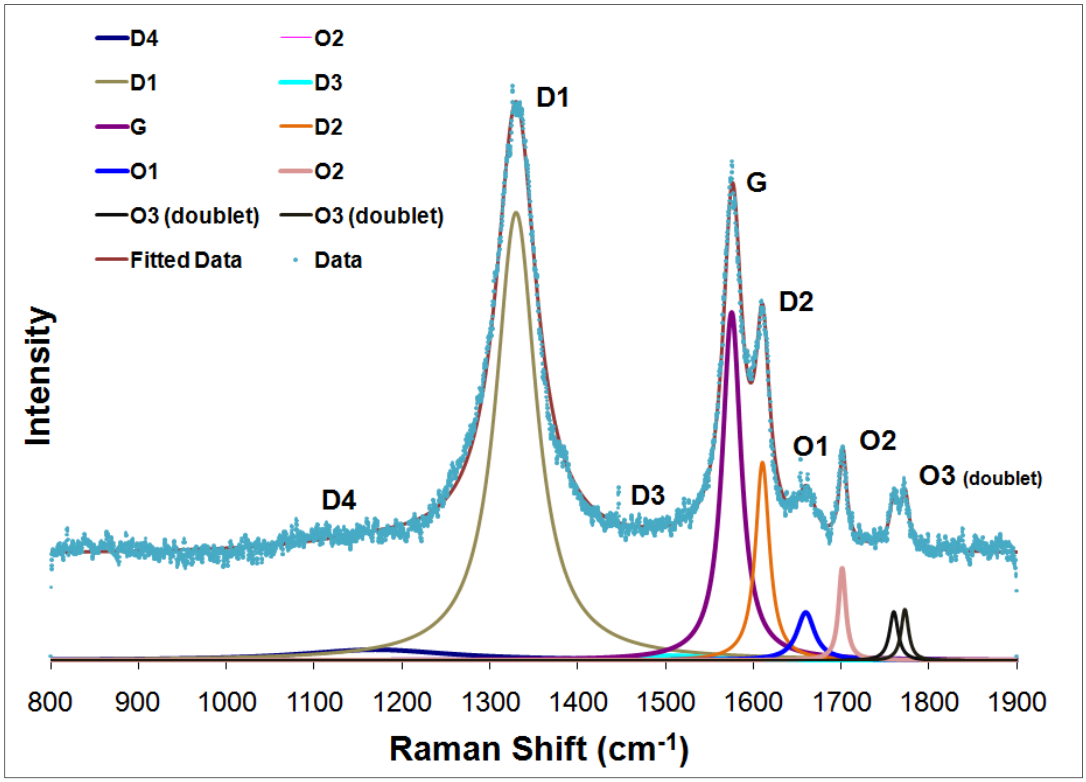

Figure VII-1: Typical Raman Spectrogram of Vapor Grown Carbon Nanofibers

The region between 800 cm^{-1} and 1630 cm^{-1} was deconvoluted into five bands, D1(Lorentzian), D2 (Lorentzian), D3 (Gaussian), D4 (Lorentzian), and G (Lorentzian) as described in the literature[59]. The G

(graphitic) peak, located at ~1570 cm^{-1} corresponds to ideal graphitic lattice vibration mode symmetry (E_{2g}). This is generally the only mode observed in highly ordered polycrystalline graphite (HOPG) whose edge lengths are longer than 100nm. The relative height and width of this band give a measure of long range two-dimensional order within the system. The largest peak on the spectra is the D1 (Disordered) band located at ~1320 cm^{-1}. The D1 band arises from carbon atoms near the edge planes of the graphene sheet[60] and does not appear in HOPG due to the lack of edge plane exposure in this system. The D1 band has been observed in spectra directed towards edge planes in large graphite single crystals. The large peak observed in all of the samples is consistent with the high edge plane exposure observed in the TEM images discussed in the next section. Several studies that the ratio of the intensities, $I_{D1}/I_{G,}$ give a quantitative measure of the degree of graphitization within the system[28, 61]. From an ORR perspective, it has been demonstrated that the D1 peak in carbon is essential for nitrogen functionalization, which, in turn, is correlated to ORR activity[22]. Table VII-2 below gives the I_{D1}/I_G of all 12 samples tested. All of the samples but one, CNF[6:4,725] have D1/G intensity ratios of greater than 1. D1 to G intensity ratios this high were not observed in any of the literature reviewed. This suggests that these CNFs have potential for nitrogen functionalization by ammonia treatment.

Table VII-1: I_{D1}/I_g Ratios for Catalysts Grown

	Catalyst Composition (*Fe:Cu*)		
Temperature(*°C*)	***6:4***	***7:3***	***8:2***
625	2.61	1.97	1.29
650	2.12	1.66	1.43
675	1.68	1.72	1.12
725	0.90	1.28	1.10

The D2 peak, observed on the shoulder of the G peak at ~1605 cm^{-1}, is, like the G peak, a result of E_{2g} vibrational mode symmetry. Raman studies of intercalated HOPG show that the D2 band completely replaces the G band . Thus, The G band represents graphene layers wedged in-between two other graphene layers, while the D2 band represents graphene layers on the surface of the fiber. A pictorial representation of geometry that gives rise to these peaks is seen in Figure VII-2 below.

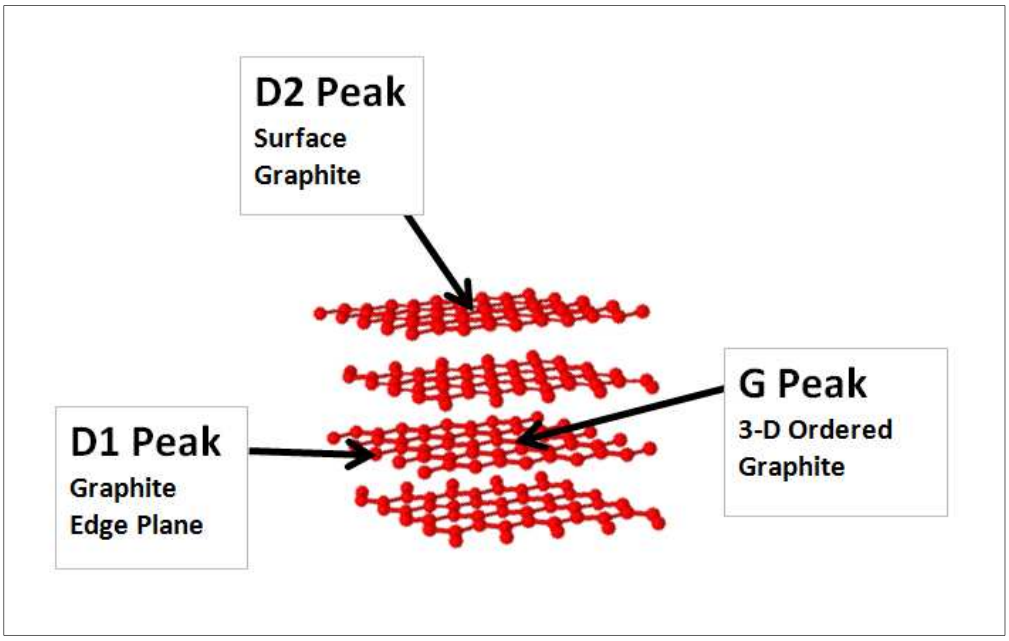

Figure VII-2: Representation of the Geometries that Cause Raman Shifts

Figure generated at: http://www.worldofmolecules.com/3D/graphite_3d.htm

The D2 bands in the samples synthesized are particularly defined as compared to similar spectra of soot[59]and carbon black[29] in which the D2 peak was only distinguished from the G peak through deconvolution. This indicates that the nanostructures of the carbons produced probably have more surface graphite compared to these other types of carbon.

The area between the D1 and G peaks that does not return to the baseline is called the D3 band. In Raman spectra of soot, this peak is much more pronounced and it is thought to correspond to

amorphous carbon[59]. The band on the shoulder of D1, denoted D4, also has been attributed to C-C and C=C stretching vibrations of polyene-like structures.

The final three bands, O1,O2,O3 (doublet) located from 1630 cm^{-1} to 1900 cm^{-1} have not yet been reported in RAMAN spectra for carboneous materials, but are repeatedly present in all unwashed and washed samples synthesized in this study. Because the samples were grown in the presence of oxygen molecules (CO), and were exposed to the atmosphere, it is reasonable to believe that oxygen heteroatoms may be present in the sample. It is postulated that carbonyl groups may be present on the edge plane of the fiber due to the presence of oxygen in the carrier gas, carbon monoxide, or by exposure to oxygen in the atmosphere. The presence of oxygen functionalities has been confirmed on N-CNFs by X-ray photoelectron spectroscopy (XPS)[25].

This claim is supported by several Raman studies of carbonyl functionalities. A doublet band corresponding to O3 located at ~1760 cm^{-1} and ~1775 cm^{-1} was observed in studies of α,β unsaturated γ-lactones[62]. Lactones present on the edge of the graphitic matrix would have very similar structure and therefore give a similar Raman band.

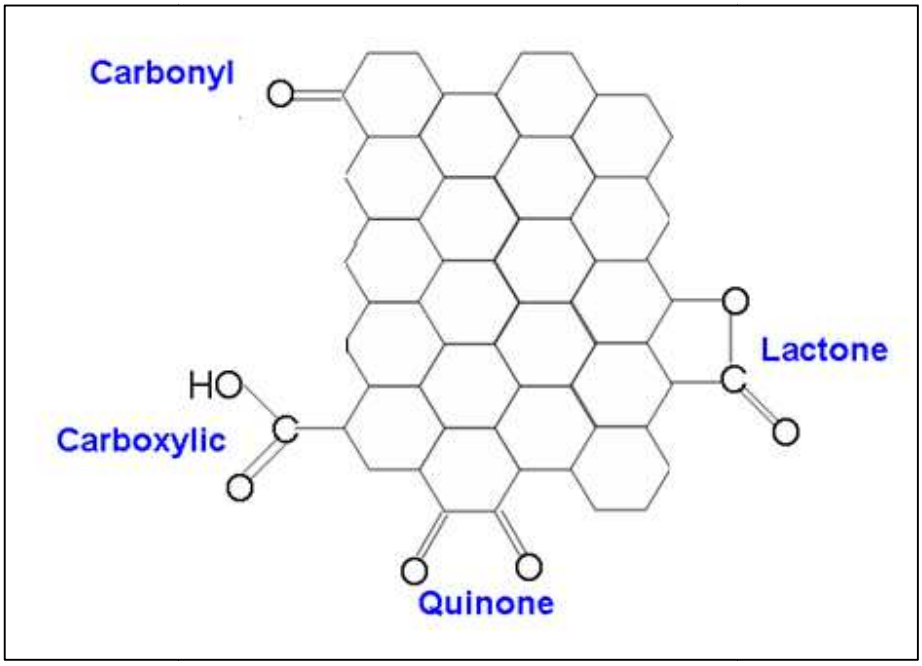

Figure VII-3: Possible Oxygen Functionalities Present on the CNFs

Image adapted from Elizabeth Biddinger

Similarly, the ortho-quinones have been observed at 1660 cm^{-1} are a probably the origin of the O1 band. Bands near the O2 (1700 cm^{-1}) vibration have been observed to correspond to unsaturated ketone (1660 cm^{-1}-1700 cm^{-1}), aldehyde (1705 cm^{-1}-1685 cm^{-1}), and carboxylic acid (1715 cm^{-1}-1690 cm^{-1}) functionalities. While further study will have to be conducted to confirm the suspected identities of the functionalities, it is clear that carbonyl functionalities do exist in these samples.

B. CNF Growth Trends

The pyrolysis of CO: H_2 (4:1) over Fe:Cu bimetallic catalysts was studied at different temperatures and the amount of carbon deposition compiled. The amount of carbon growth varied

greatly though the experiments with the highest amount being 14.7 times the initial catalyst mass CNF[8:2,675°C]and the lowest just over 2 times the catalyst mass CNF[8:2, 725°C]. Figure VII-4 shows a reduction of growth occurs at 725°C for all three formulations. The 8:2 Fe:Cu catalyst showed the most deactivation (7-fold reduction in deposition) while the 6:4 catalyst showed the least (just over 2 times less).

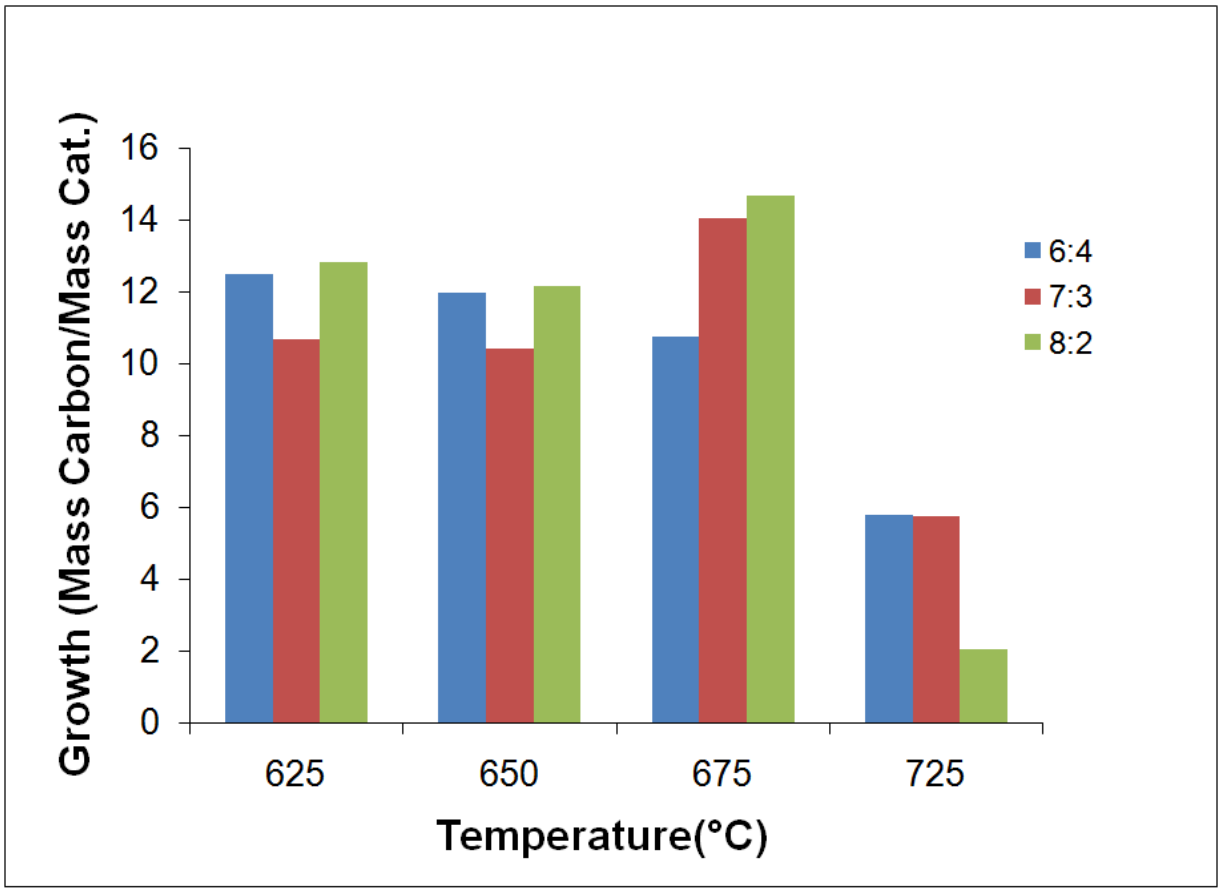

Figure VII-4: Carbon Deposition of CO/H_2 over Bimetallic Fe:Cu Catalysts at Various Temperatures.

Evidence for deactivation was observed in TEM images taken of the CNF [8:2 725°C] sample.

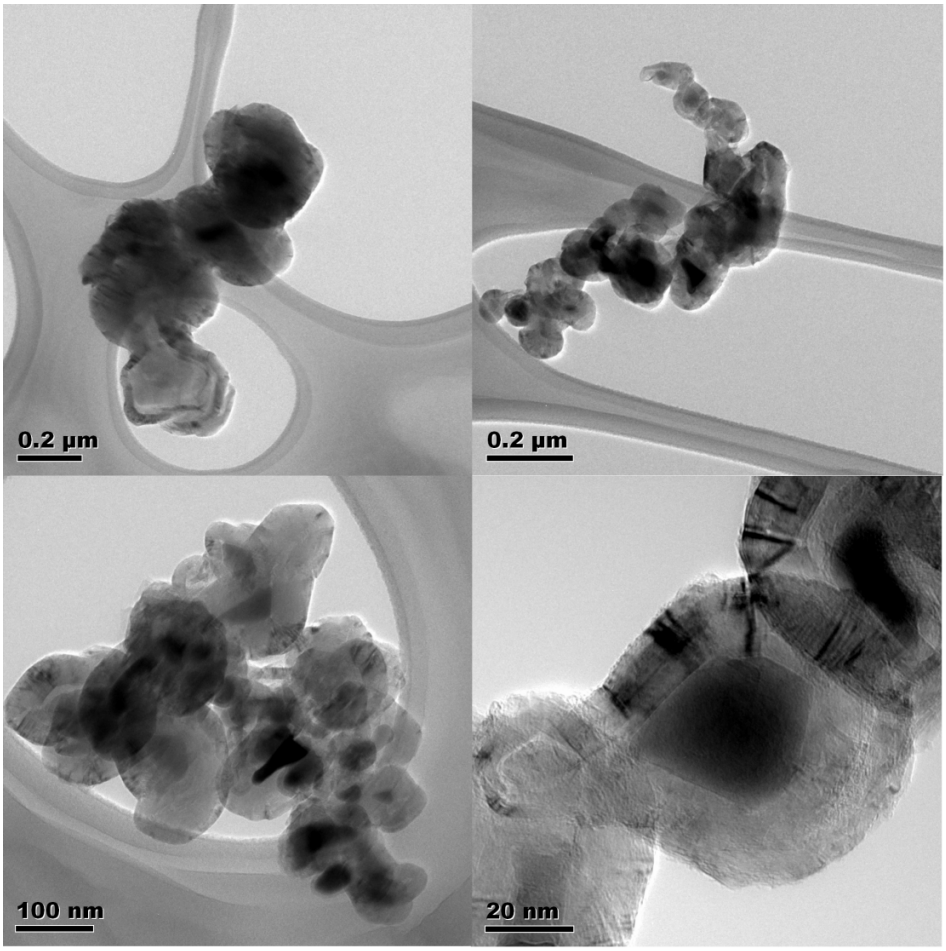

Figure VII-5: 8:2 Fe:Cu Deactivation at 725◦C by Carbon Encapsulation.

At this temperature, there appears to be an increase in metallic particles (darker areas) encapsulated by carbon compared to growth at lower temperatures and a decrease in fibrous nanocarbons. Literature suggests that in order for the catalyst to be active for carbon deposition some portion of the surface must be exposed. It has been suggested that the reason for growth catalyst encapsulation is a change in surface chemistry of the metal particle[33].

Analysis of Figure VII-4 reveals that 8:2 Fe: Cu catalysts show the most growth in the active range (625°C-675°C), but activity falls off sharply at 725°C. Also, 6:4 Fe:Cu catalysts show a reduction in growth as temperature is increased, but this is not seen in other catalyst formulations. The reason for these two trends is still being investigated.

C. Morphological Characterization

9 of the 12 CNFs grown were characterized as either platelet or multi-walled nanotubes (MWNTs), Figure VII-6(A) shows that the MWNTs have are have vertically aligned structures wrapped around a hollow core. In contrast, the platelet type has clearly shown horizontal stacking of the graphitic planes.

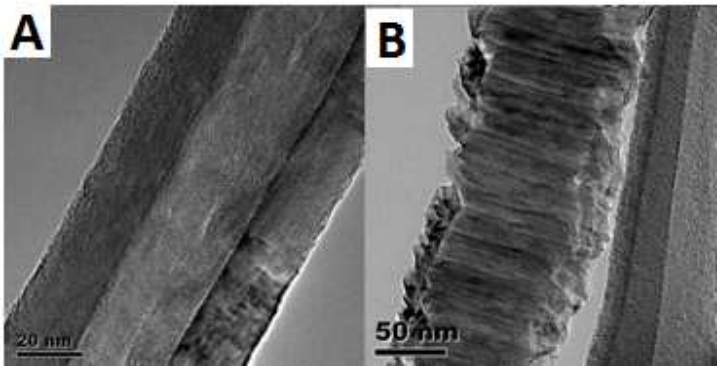

Figure VII-6: TEM images of (A) a MWNT and (B) a Platelet Nanofiber

Images Courtesy of Elizabeth Biddinger

The CNF[8:2, 625°C], CNF[8:2, 650°C] and CNF[7:3,650°C] samples do not appear to have any easily recognizable structures. CNF[8:2,625°C] appears to be composed of twisted fibers with graphene sheets twisting around a growth axis. There is also evidence of thick, disordered fibers. CNF[8:2,650°C] is very heterogeneous with convoluted and distorted nanostructures. CNF[7:3,650°C] is composed of

vertically- aligned CNFs that appear to look like flattened MWNTs. Flattened MWNTs have been observed elsewhere[63]. They attributed flattening to pressure differences between the inside and outside of the tube caused by sealing of a MWNT during growth.

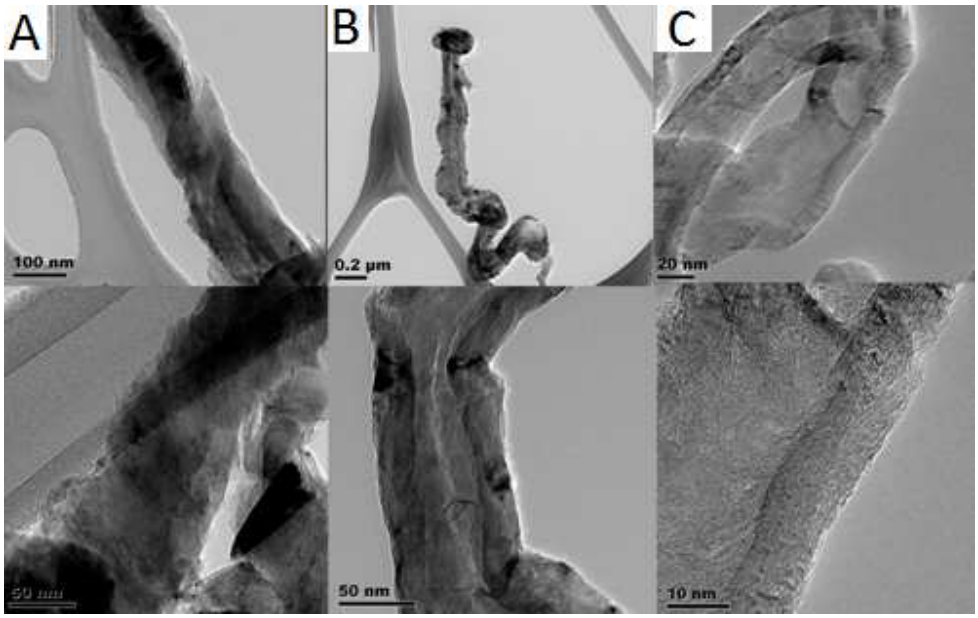

Figure VII-7: TEM Images of (A) CNF [8:2,625°C], (B), CNF [8:2, 650°C], (C),CNF[7:3, 650°C]

Images Courtesy of Elizabeth Biddinger

An attempt was made to study the relative effect of temperature and growth catalyst composition on final CNF morphology. Figure VII-8 shows TEM images of the CNFs organized in a matrix of temperature and catalyst compositions.

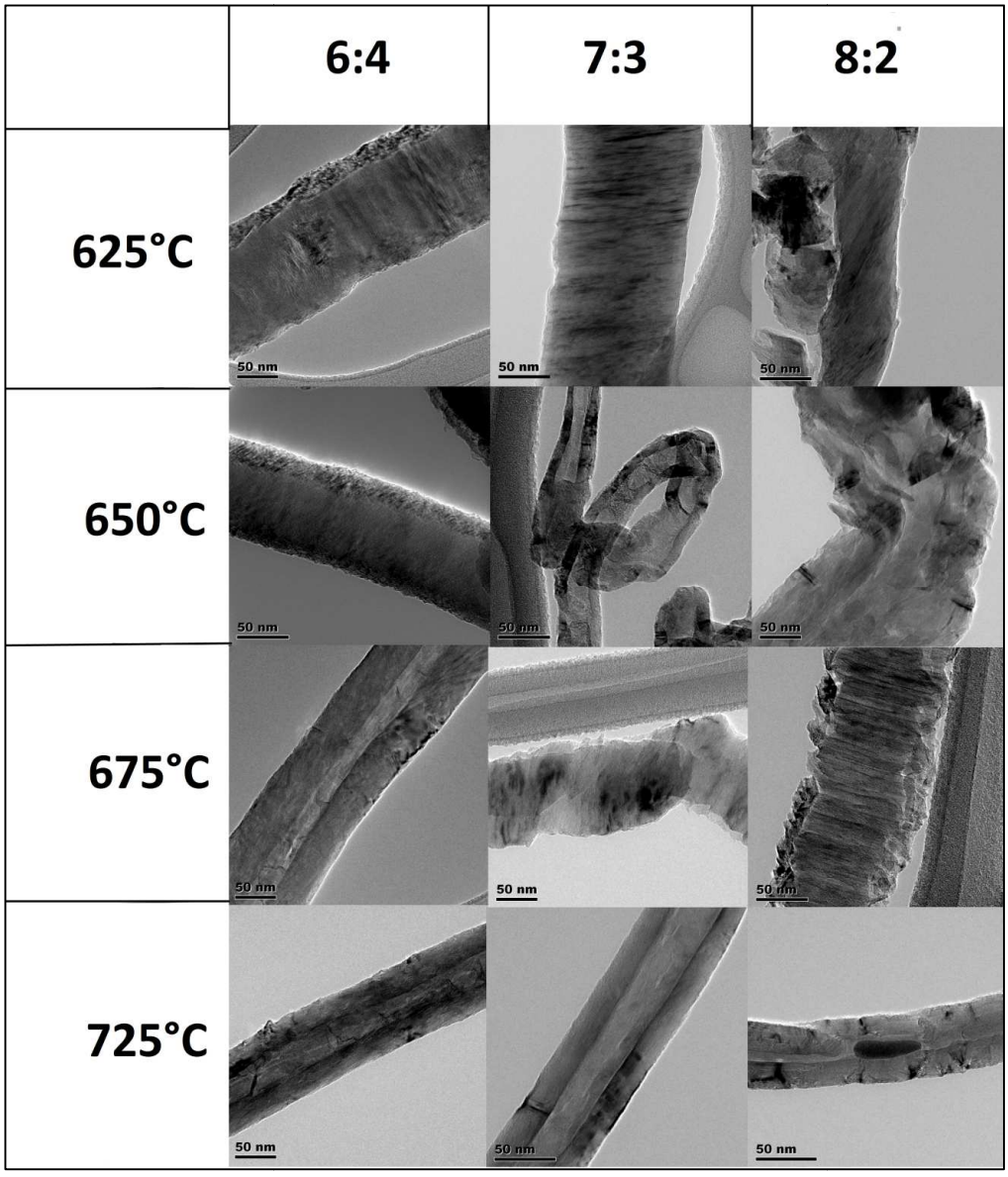

Figure VII-8: Temperature and Catalyst Effects on Final CNF Morphology

Images Courtesy of Elizabeth Biddinger

Platelet type nanofibers were the most commonly observed morphology. They appear at lower temperatures and lower iron content (CNF[6:4,625°C], CNF[6:4; 650°C], CNf[7:3, 625°C]) and reemerge at 675°C. (CNF[7:3, 675°C], CNF[8:2, 675°C]). As temperature rises there appears to be a tendency for

CNFs to form the MWNT morphology. In each of the 725°C samples MWNTs are seen dispersed with the deactivated carbon encapsulated metal particles. Interestingly, the 6:4 Fe:Cu grown samples appear to go through a fundamental morphological shift from platelet to tubule structure between 650°C and 675°C. This is also true for 8:2 and 7:3 Fe:Cu formulations between 675°C and 725°C. A similar morphological shift was observed by Carneiro in the study of Fe:Cu catalysts[33]. This change was attributed to a shift in the crystalline structure of iron from α-Fe (body-centered cubic) to γ-Fe (face-centered cubic). This phase change is known to occur at 727°C in an iron-carbon system at less than 5 wt% carbon[64].

In general, it is hard to clearly discern the temperature and growth catalyst effects from these TEM images. This could be because they represent such a small portion of the sample and the part examined is not represented by the bulk. Because of this, further experiments were done to confirm the morphologies observed in the TEM images. The CNFs were dispersed in water to get an idea of their relative hydrophobicity. As noted in the introduction, platelet nanofibers tend to be more hydrophilic and will disperse more easily in water. Figure VII-9 shows the 6:4 Fe:Cu grown samples organized from low to high growth temperatures.

Figure VII-9: 6:4 Fe:Cu Samples Organized From Low to High Temperature

The high dispersion of CNF[6:4,625°C] and CNF[6:4,650°C] support the assertion that these two samples are composed primarily of platelet CNFs, whereas the low dispersion in the high temperature samples indicates they are made up of a more hydrophobic carbon such as MWNTs. Hydrophobicity testing on the other samples showed that the platelet nanofibers were generally more dispersive than non-platelets, but the 6:4 Fe: Cu platelets were the most dispersive.

The 6:4 Fe: Cu samples were further analyzed by Raman analysis. I_{D1}/I_G peaks in these samples give an indication of the level of edge plane exposure to graphite in the particles. Figure VII-10 shows the the I_{D1}/I_G for the 6:4 samples. There appears to be a reduction of edge planes to graphite in these samples. This is expected because MWNTs have less edge plane exposure. On average the samples characterized as platelets had an I_{D1}/I_G ratio of 2.07 and a standard deviation of 0.334 while the MWNTs had an average of 1.30±0.35 (standard deviation).

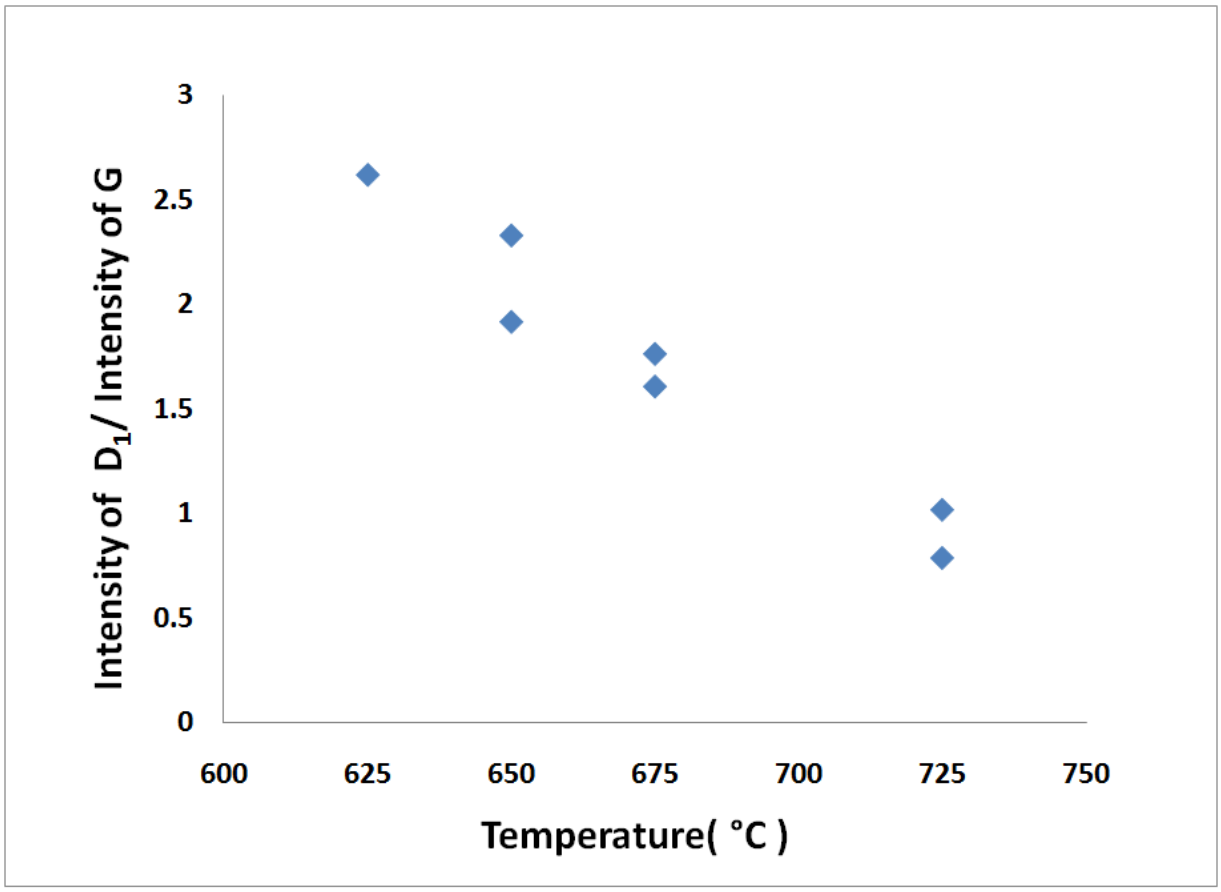

Figure VII-10: The Ratio of Intensities between the G and D1 peaks versus Temperature in the 6:4 Grown Samples

VIII. Results and Discussion - Thiophene in N-CNF Synthesis

A. Growth Effects

Thiophene(C_4H_4S) was added to the acetonitrile (CH_3CN) reactant stream in varying concentrations to study its effect on N-CNF growth. The amount of carbon deposition, reported as a percentage of catalyst weight, vs. mole% thiophene in acetonitrile can be seen in Figure VIII-1.

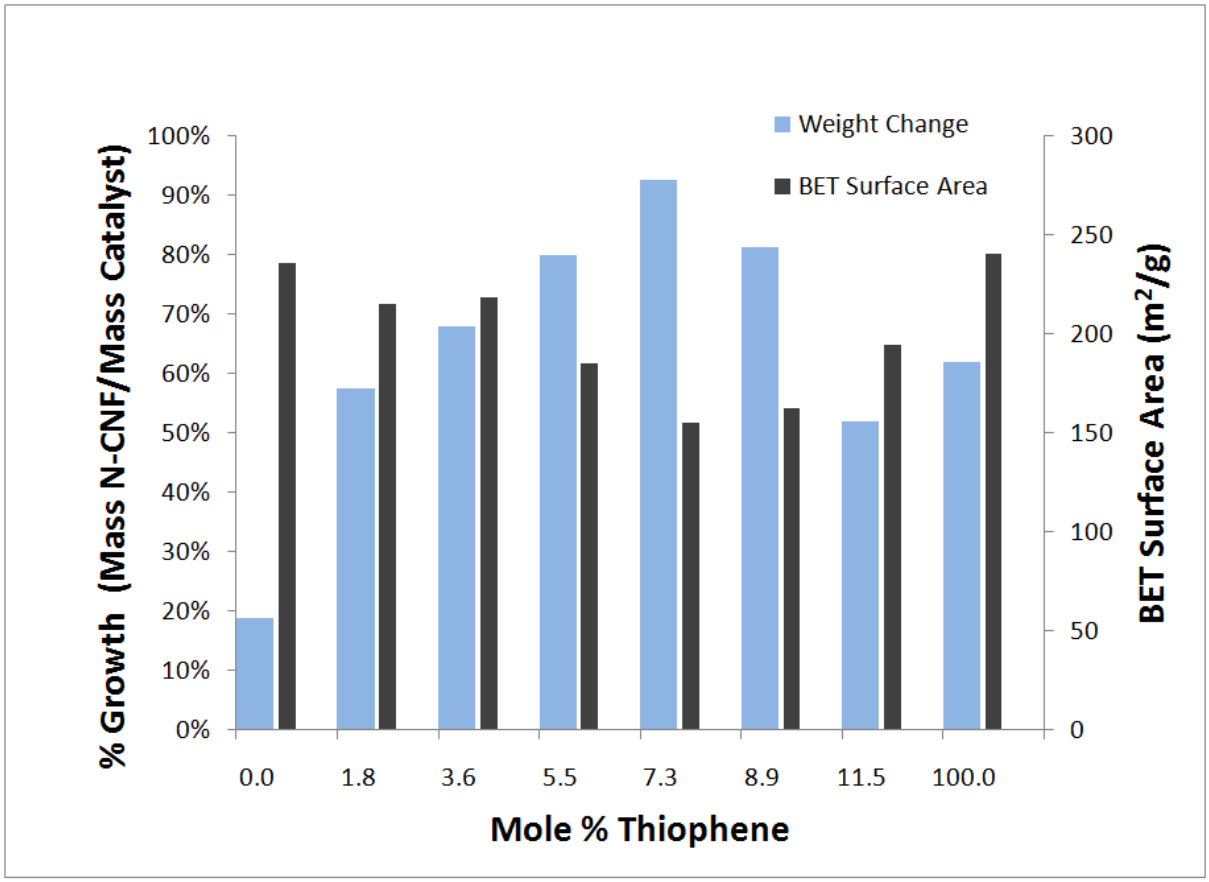

Figure VIII-1: Weight Gain (Y_1) and BET Surface Area(Y_2) vs. Thiophene in the Pyrolysis of Acetonitrile over 2% Fe/MgO at 900°C

Thiophene does act as a growth promoter in acetonitrile pyrolysis. Moreover, CVD mass increases with increasing thiophene concentration until 7.3%, where it begins to decline. The observed increase in carbon deposition and associated maxima are consistent with the observations of several researchers studying the growth of non-nitrogen containing CNFs discussed earlier in the literature review. Surprisingly, carbon pyrolysis of pure thiophene yields more carbon growth than pure acetonitrile, 1.8% thiophene and 11.5% thiophene. This observation is problematic for both proposed sulfur growth promotion mechanisms. Kim *et al.* suggests that at high concentrations, adsorbed sulfur blocks carbon deposition[55]. This assertion is supported by the observed decrease in deposition at 8.9% and 11.5% thiophene, but fails to explain the deposition at 100% thiophene. Similarly, the maxima at 7.2% thiophene could support Tibbets and coworkers proposed mechanism that proximity to the eutectic and deposition through vapor-liquid-solid mechanism is the reason for sulfur growth promotion[58]. It also fails to explain why there is more deposition of pure thiophene than 8.9% thiophene, which whose composition is presumably closer to the eutectic. This may indicate that carbon deposition proceeds by a different pathway in thiophene growth.

The inverse relationship between BET surface area and growth is also shown on Figure VIII-1. It was observed that nanofibers with higher growth rates showed a decrease in surface area. This is likely due to a shift in bulk nanostructure morphology or by coverage of micropores by low surface area, bulk carbon.

B. Morphological Effects

TEM images taken by Elizabeth Biddinger show that the N-CNF nanofibers grown with pure acetonitrile are composed primarily of stacked-cup nanofibers and nanocubes. The fiber structure of fibers grown with pure acetonitrile and 1.8% thiophene in acetonitrile can be seen in Figure VIII-2 below.

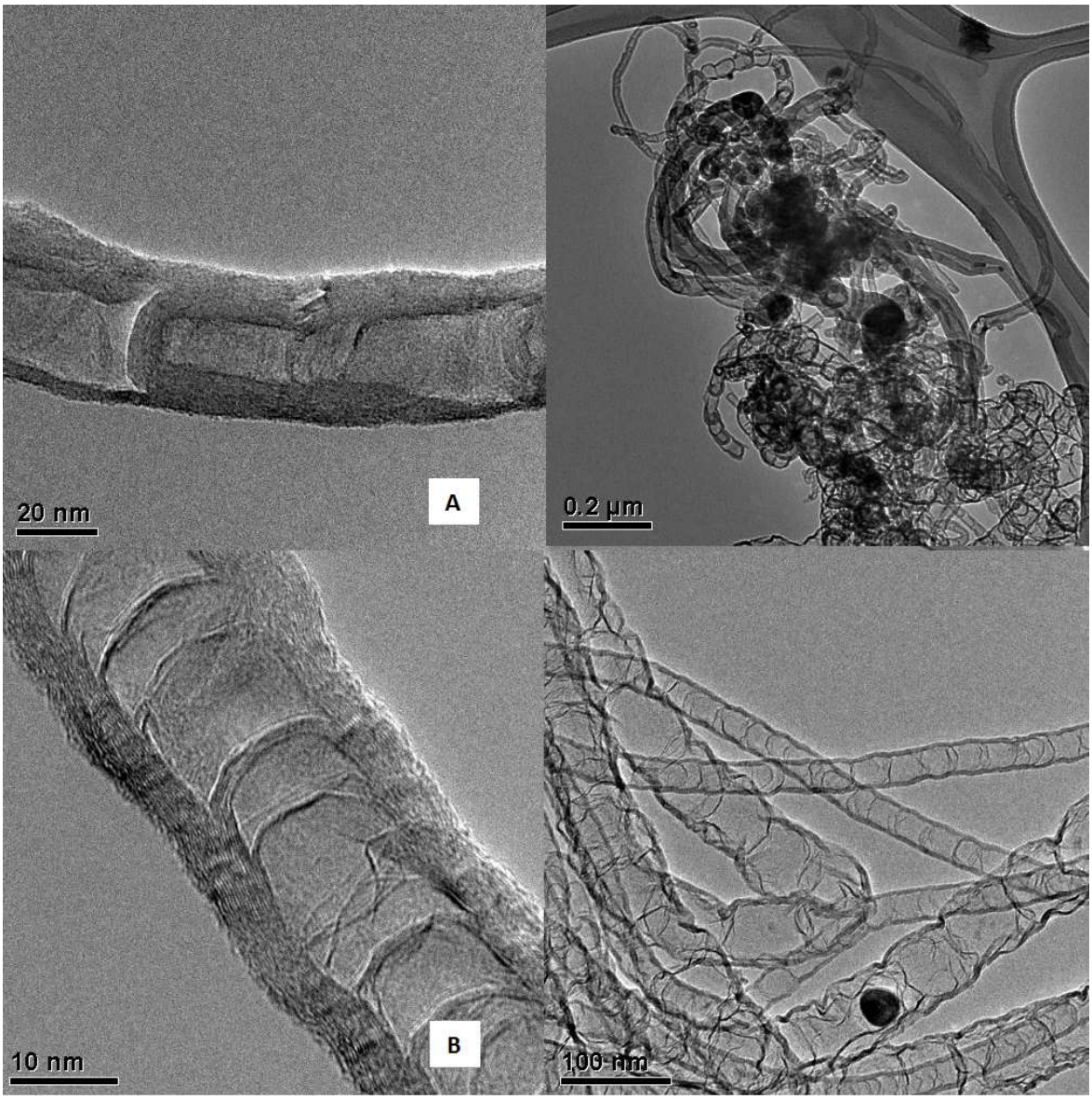

Figure VIII-2: N-CNFs Grown with (A) Pure acetonitrile and (B) 1.8% Thiophene

Images Courtesy of Elizabeth Biddinger

This is consistent with results presented in several publications for nanofibers grown at 900°C over Fe catalysts [65-67]. They consist of stacked cup type nanofibers with edge plane exposure on the lip of each stacked cup. There is morphological similarity between the pure acetonitrile and 1.8% thiophene samples. In contrast, Figure VIII-3 shows the TEM images of samples at grown with 11.5% thiophene (A) and pure thiophene(B).

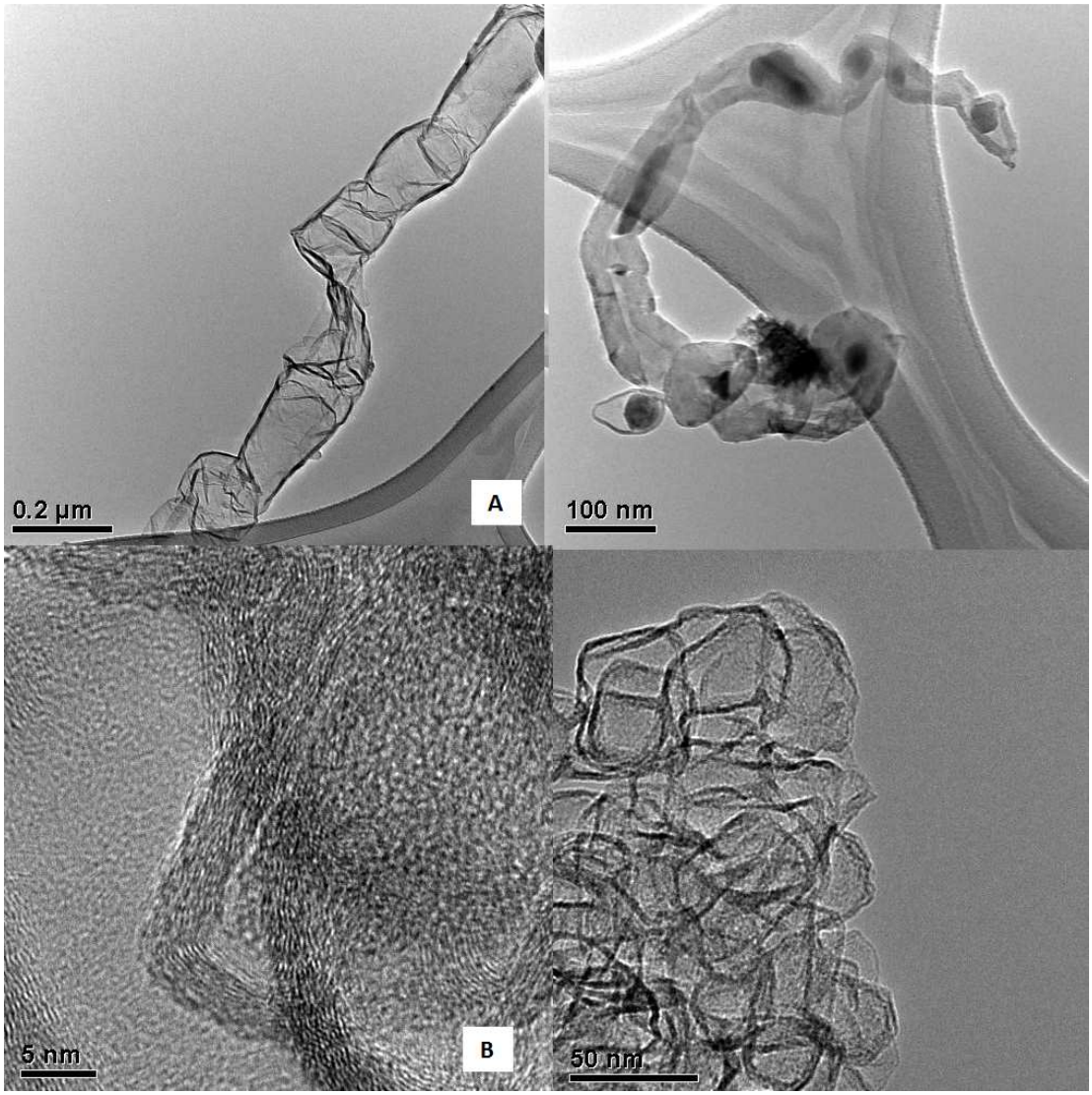

Figure VIII-3: CNFs Grown with (A) 11.5% Thiophene and (B) Pure Thiophene.

Images Courtesy of Elizabeth Biddinger

Figure VIII-3(A) is indicative of the nanostructures observed in samples grown with higher levels of thiophene. They appear to be made up of more disordered stacked cup structures and have a lower proportion of long, pristine fibers. The samples grown in pure thiophene are made up of pure cubic nanostructures, with no indication of long fibers characteristically observed in acetonitrile pyrolysis.

It was asserted that the breakup of the graphitic matrix in the thiophene/acetonitrile samples was caused by disruption to the graphitic matrix by sulfur heteroatoms. To test this, temperature programmed oxidations (TPO) of the samples were performed and the resulting gas analyzed by a mass spectrometer[25]. These TPOs indicated that both the thiophene and non-thiophene grown fibers show evidence of carbon and nitrogen in during oxidation. In addition, the thiophene samples show that after desorption of sulfur at 175°C, there is a sulfur signal detected during the oxidation of the fiber itself. This confirms that sulfur is present in the graphitic matrix in the thiophene grown samples. Further investigation of the desorption, oxidation, and structural properties of these nanofibers were recently published[25].

C. Catalytic Effects

Although increased fiber growth is advantageous from a production perspective, the decreased surface area and presence of sulfur could have negative effects on the ORR activity in fuel cells. Surface area reduction is often correlated to decreased catalytic performance because there is less physical space for the active sites to reside. Additionally, sulfur is known to be a poison in multiple catalysts systems including fuel cells[68].

RRDE testing was performed to test the catalytic effect of thiophene growth promotion on N-CNFs. Figure VIII-4 shows a representative cyclic voltammogram of a pure thiophene, acetonitrile/thiophene, and acetonitrile N-NCFs.

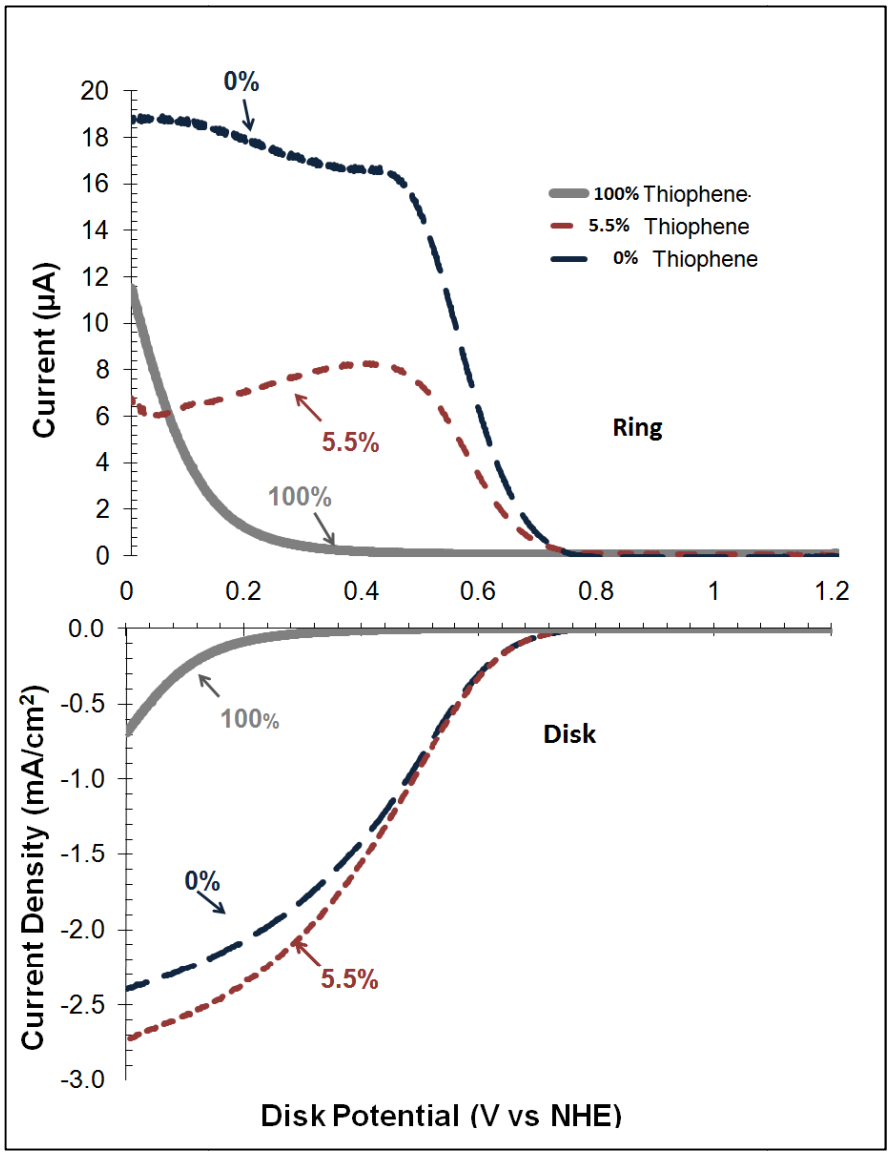

Figure VIII-4: Selected Cyclic Voltammograms of N-CNF Catalysts

The N-CNF grown with acetonitrile only had an onset of activity of 760 mV. N-CNFs made from the thiophene/acetonitrile mixtures had onset of activities near that of acetonitrile only N-CNF. The thiophene-only sample shows very little activity, only separating at 510 mV. Oxygen is either reduced to H_2O (preferred) or H_2O_2. When it is reduced to H_2O_2, current is detected on the ring (top half) and selectivity can be determined from this value.

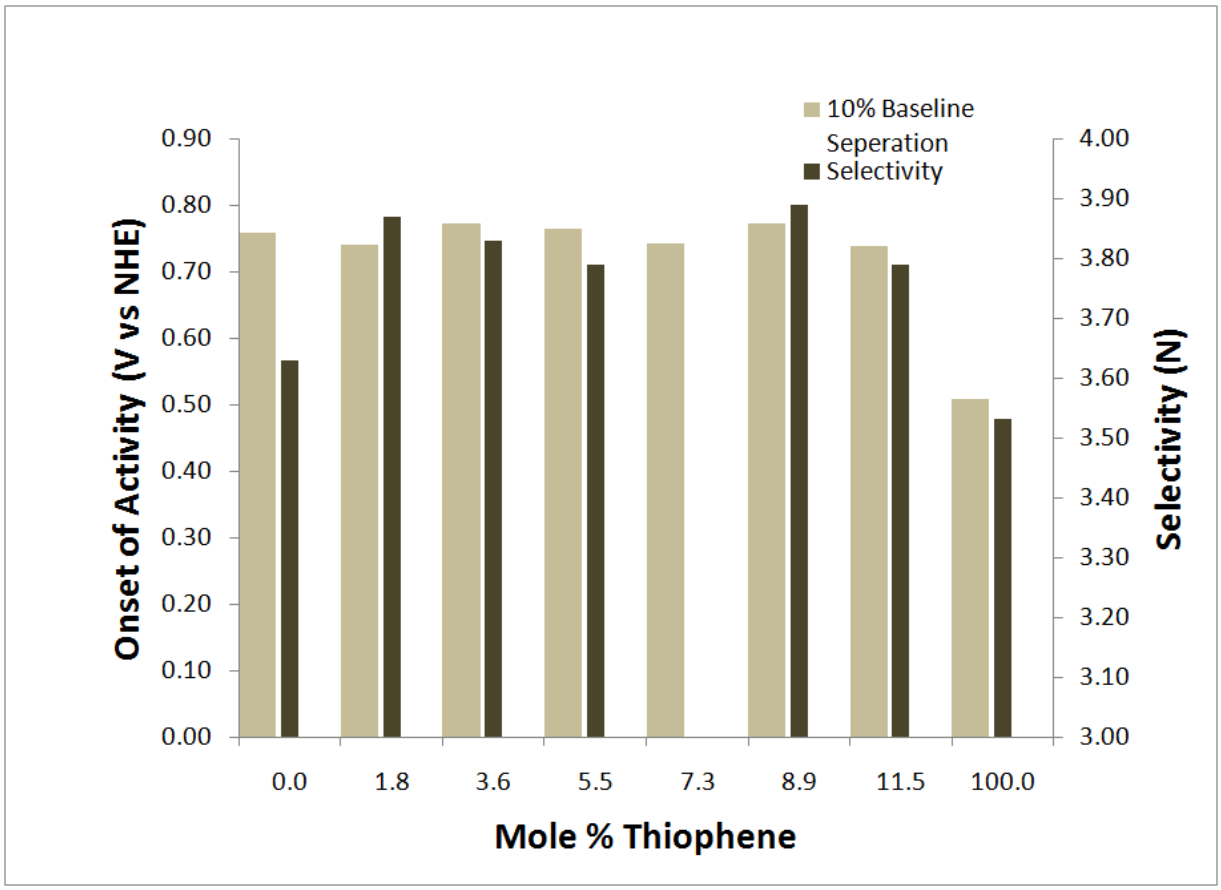

Figure VIII-5: Onset of Activity and Selectivity at 0.60 V Vs. Thiophene in the Acetonitrile Bubbler

The results indicate that the onset of activity of the N-CNFs remain constant up to 11.5% thiophene, while the pure thiophene sample shows little activity. Selectivity does not seem to be influenced.

IX. Conclusions

Two experimental sets were conducted that studied the growth of carbon nanofibers for eventual use as ORR catalysts. In one study, thiophene was added to acetonitrile pyrolysis in varying amounts to determine the growth, morphological, and ORR catalytic effect of such an addition. It was determined that increasing thiophene concentration causes increased carbon deposition until 7.3 mol % thiophene after which growth declines. Pure thiophene grown samples also caused carbon deposition. As thiophene levels increased TEM revealed a morphological shift from pristine stacked cups to a more disordered stacked cup conformation. TPOs of the nanofibers confirm this, and show that sulfur is being incorporated into the graphitic matrix[25]. RRDE half cell testing shows that the increased growth and morphological shift have no effect on N-CNF catalytic activity. Thus, it is concluded that industrial scale growth of these N-CNFs could benefit from thiophene addition and not suffer from performance degradation.

In another study, the effects of variation in temperature and growth catalyst composition were studied in the deposition of $CO:H_2$ (4:1).The resulting nanofibers were evaluated for nitrogen functionalization potential. For all catalyst formulations studied, partial catalyst deactivation was observed for samples grown at 725°C as indicated by growth reduction and the occurrence of graphite-encapsulated metal particles. Platelet nanofibers were the most common fibers grown, and several other more complex nanostructures observed. Hydrophobicity testing, Raman analysis, and TEM images of the nanofibers grown using the 6:4 Fe:Cu catalyst indicate a morphological shift from platelet to MWNT nanostructure between 650°C and 675°C possibly indicating a change from α-Fe to γ-Fe. This shift is observed from 675°C to 725°C in other two catalysts. Raman spectrograms showed evidence of oxygen surface functionalities on the surface of the nanofiber. In addition, Raman spectroscopy

revealed that all of the fibers have large D1/G Intensity ratios indicating they have potential for ammonia functionalization and later use.

X. Opportunity for Further Study

The results presented in this thesis highlight the need for further study on several fronts. Firstly, the CNFs generated in the deposition of $CO:H_2$ (4:1) over bimetallic catalysts could be further characterized. They could be tested for surface area and pore volume to get a better idea of how these carbon CNFs compare to other types of carbon, such as carbon black and graphite. Also, characterization could be done to determine the exact nature of oxygen functionalities observed on the surface of the CNF in Raman spectroscopy and reported. This could be achieved through X-ray photoelectron spectroscopy (XPS), Temperature Programmed Desorption coupled with mass spectrometry and in-situ Raman under reduction conditions. In addition, the Iron/Copper growth catalysts could be further characterized to determine the particle size and composition of each catalyst to better understand the growth trends observed. In regards to ORR catalysis, the samples containing the highest I_{D1}/I_G peaks could be functionalized with nitrogen and tested for onset of activity and selectivity in RRDE.

Bibliography

1. Kemp, R., J. Schot, and R. Hoogma, *Regime shifts to sustainability through processes of niche formation: The approach of strategic niche management.* Technology Analysis & Strategic Management, 1998. **10**(2): p. 175 - 198.
2. Watkins, G.C., *Oil scarcity: What have the past three decades revealed?* Energy Policy, 2006. **34**(5): p. 508-514.
3. Basher, S.A. and P. Sadorsky, *Oil price risk and emerging stock markets.* Global Finance Journal, 2006. **17**(2): p. 224-251.
4. Bard, A.J. and L.R. Faulkner, *Electrochemical methods: fundamentals and applications*. 2001, New York: John Wiley and Sons Ltd.
5. Bonakdarpour, A., T.R. Dahn, R.T. Atanasoski, M.K. Debe, and J.R. Dahn, *H_2O_2 release during oxygen reduction reaction on Pt nanoparticles.* Electrochemical and Solid-State Letters, 2008. **11**: p. B208-B211.
6. Gasteiger, H.A., J.E. Panels, and S.G. Yan, *Dependence of PEM fuel cell performance on catalyst loading.* Journal of Power Sources, 2004. **127**: p. 162-171.
7. Masten, D.A. and A.D. Bosco, *System design for vehicle applications: GM/Opel*, in *Handbook of Fuel Cells - Fundamentals, Technology and Applications*, W. Vielstich, A. Lamm, and H.A. Gasteiger, Editors. 2003, John Wiley & Sons, Ltd. p. 714.
8. Vielstich, W., H.A. Gasteiger, and A. Lamm, eds. *Handbook of Fuel Cells - Fundamentals, Technology and Applications*. Vol. 2: Electrocatalysis. 2003, John Wiley & Sons, Ltd.
9. Johnson Matthey Precious Metals Marketing. *Platinum Today*. 2010 [cited 2008; Available from: http://www.platinum.matthey.com/index.html.
10. Jasinski, R., *Cobalt phthalocyanine as a fuel cell cathode.* Journal of the Electrochemical Society, 1965. **112**(5): p. 526-528.
11. Jasinski, R., *A new fuel cell cathode catalyst.* Nature, 1964. **201**: p. 1212.
12. Jahnke, H., M. Schonborn, and G. Zimmerman, *Organic dyestuffs as catalysts for fuel cells.* Fortschr. Chem. Forsch., 1976. **61**: p. 133.
13. Lefevre, M., J.P. Dodelet, and P. Bertrand, *Molecular oxygen reduction in PEM fuel cells: Evidence for the simultaneous presence of two active sites in Fe-based catalysts.* Journal of Physical Chemistry B, 2002. **106**: p. 8705-8713.
14. Jaouen, F., M. Lefevre, J.-P. Dodelet, and M. Cai, *Heat-treated Fe/N/C catalysts for O_2 electroreduction: Are active sites hosted in micropores?* Journal of Physical Chemistry B, 2006. **110**: p. 5553-5558.
15. Wiesener, K., *N_4-chelates as electrocatalysts for cathodic oxygen reduction.* Electrochimica Acta, 1986. **31**(8): p. 1073-1078.
16. Matter, P.H. and U.S. Ozkan, *Non-metal catalysts for dioxygen reduction in an acidic electrolyte.* Catalysis Letters, 2006. **109**(3-4): p. 115-123.
17. Matter, P.H., L. Zhang, and U.S. Ozkan, *The role of nanostructure in nitrogen-containing carbon catalysts for the oxygen reduction reaction.* Journal of Catalysis, 2006. **239**: p. 83-96.
18. Matter, P.H., E. Wang, M. Arias, E.J. Biddinger, and U.S. Ozkan, *Oxygen reduction reaction catalysts prepared from acetonitrile pyrolysis over alumina supported metal particles.* Journal of Physical Chemistry B, 2006. **110**: p. 18374-18384.

19. Matter, P.H., E. Wang, M. Arias, E.J. Biddinger, and U.S. Ozkan, *Oxygen reduction reaction activity and surface properties of nanostructured nitrogen-containing carbon.* Journal of Molecular Catalysis, 2007. **264**(1-2): p. 73-81.
20. Matter, P.H., E. Wang, and U.S. Ozkan, *Preparation of nanostructured nitrogen-containing carbon catalysts for the oxygen reduction reaction from SiO_2 and MgO supported metal particles.* Journal of Catalysis, 2006. **243**: p. 395-403.
21. Lefevre, M. and J.-P. Dodelet, *Fe-based electrocatalysts made with microporous pristine carbon black supports for the reduction of oxygen in PEM fuel cells.* Electrochimica Acta, 2008. **53**: p. 8269-8276.
22. Jaouen, F., F. Charreteur, and J.P. Dodelet, *Fe-based catalysts for oxygen reduction in PEMFCs: Importance of the disordered phase of the carbon support.* Journal of the Electrochemical Society, 2006. **153**: p. A689-A698.
23. Ozaki, J.-i., N. Kimura, T. Anahara, and A. Oya, *Preparation and oxygen reduction activity of BN-doped carbons.* Carbon, 2007. **45**: p. 1847-1853.
24. Liu, H., Y. Zhang, R. Li, X. Sun, S. Desilets, H. Abou-Rachid, M. Jaidann, and L.-S. Lussier, *Structural and morphological control of aligned nitrogen-doped carbon nanotubes.* Carbon, 2010. **48**: p. 1498-1507.
25. Biddinger, E.J., D.S. Knapke, D. von Deak, and U.S. Ozkan, *Effect of sulfur as a growth promoter for CN_x nanostructures as PEM and DMFC ORR catalysts.* Applied Catalysis B: Environmental, 2010. **96**: p. 72-82.
26. De Jong, K.P. and J.W. Geus, *Carbon nanofibers: catalytic synthesis and applications.* Catalysis Reviews: Science and Engineering, 2000. **42**(4): p. 481 - 510.
27. Herranz, J., F. Jaouen, and J.-P. Dodelet, *Electrochemical evidence of two types of active sites for oxygen reduction in Fe-based catalysts.* ECS Transactions, 2009. **25**: p. 117-128.
28. Chieu, T.C., M.S. Dresselhaus, and M. Endo, *Raman studies of benzene-derived graphite fibers.* Physical Review B, 1982. **26**: p. 5867-5877.
29. Charreteur, F., F. Jaouen, S. Ruggeri, and J.-P. Dodelet, *Fe/N/C non-precious catalysts for PEM fuel cells: Influence of the structural parameters of pristine commercial carbon blacks on their activity for oxygen reduction.* Electrochimica Acta, 2008. **53**: p. 2925-2938.
30. Rodriguez, N.M., *A review of catalytically grown carbon nanofibers.* Journal of Materials Research, 1993. **8**(12): p. 3233-3250.
31. Baker, R.T.K. and N.M. Rodriguez, *Process for production of crystalline graphite nanofibers*, in *U.S. Pat. Appl. Publ.* 2002, (USA). Us. p. 8 pp., Cont.-in-part of U.S. 659,441.
32. Carneiro, O.C., P.E. Anderson, N.M. Rodriguez, and R.T.K. Baker, *Decomposition of CO-H_2 over graphite nanofiber-supported iron and iron-copper catalysts.* Journal of Physical Chemistry B, 2004. **108**(35): p. 13307-13314.
33. Carneiro, O.C., M.S. Kim, J.B. Yim, N.M. Rodriguez, and R.T.K. Baker, *Growth of graphite nanofibers from the iron-copper catalyzed decomposition of CO/H_2 mixtures.* Journal of Physical Chemistry B, 2003. **107**(18): p. 4237-4244.
34. Lefevre, M., E. Proietti, F. Jaouen, and J.-P. Dodelet, *Iron-based catalysts with improved oxygen reduction activity in polymer electrolyte fuel cells.* Science, 2009. **324**: p. 71-74.
35. Kim, M.S., N.M. Rodriguez, and R.T.K. Baker, *The interplay between sulfur adsorption and carbon deposition on cobalt catalysts.* Journal of Catalysis, 1993. **143**: p. 449-463.
36. Fan, Y.-Y., H.-M. Cheng, Y.-L. Wei, G. Su, and Z.-H. Shen, *The influence of preparation parameters on the mass production of vapor-grown carbon nanofibers.* Carbon, 2000. **38**: p. 789-795.
37. Ci, L., Y. Li, B. Wei, J. Liang, C. Xu, and D. Wu, *Preparation of carbon nanofibers by the floating catalyst method.* Carbon, 2000. **38**: p. 1933-1937.

38. Baker, R.T.K., M.A. Barber, P.S. Harris, F.S. Feates, and R.J. Waite, *Nucleation and growth of carbon deposits from the nickel catalyzed decomposition of acetylene.* Journal of Catalysis, 1972. **26**: p. 51-62.
39. Melechko, A.V., V.I. Merkulov, T.E. McKnight, M.A. Guillorn, K.L. Klein, D.H. Lowndes, and M.L. Simpson, *Verically aligned carbon nanofibers and related structures: Controlled synthesis and directed assembly.* Journal of Applied Physics, 2005. **97**.
40. Sacco, A., P. Thacker, T.N. Chang, and A.T.S. Chiang, *The initiation and growth of filamentous carbon from α-iron in H_2, CH_4, H_2O, CO_2, and CO gas mixtures.* Journal of Catalysis, 1984. **85**: p. 224-236.
41. Boellaard, E., P.K. de Boxx, A.J.H.M. Kock, and J.W. Geus, *The formation of filamentous carbon on iron and nickel catalysts.* Journal of Catalysis, 1985. **96**: p. 481-490.
42. Alstrup, I., *A new model explaining carbon filament growth on nickel, iron, and Ni-Cu alloy catalysts.* Journal of Catalysis, 1988. **109**: p. 241-251.
43. Snoeck, J.W., G.F. Froment, and M. Fowles, *Filamentous carbon formation and gasification: Thermodynamics, driving force, nucleation, and steady-state growth.* Journal of Catalysis, 1997. **169**(1): p. 240-249.
44. Tesner, P.A., E.Y. Robinovich, I.S. Rafalkes, and E.F. Arefieva, *Formation of carbon fibers from acetylene.* Carbon, 1970. **8**(4): p. 435-440, IN1-IN2, 441-442.
45. Helveg, S., C. Lopez-Cartes, J. Sehested, P.L. Hansen, B.S. Clausen, J.R. Rostrup-Nielsen, F. Abild-Pedersen, and J.K. Norskov, *Atomic-scale imaging of carbon nanofibre growth.* Nature, 2004. **427**(6973): p. 426-429.
46. Carneiro, O.C., N.M. Rodriguez, and R.T.K. Baker, *Growth of carbon nanofibers from the iron-copper catalyzed decomposition of CO/C2H4/H2 mixtures.* Carbon, 2005. **43**(11): p. 2389-2396.
47. Rodriguez, N.M., M.S. Kim, and R.T.K. Baker, *Promotional effect of carbon monoxide on the decomposition of ethylene over an iron catalyst.* Journal of Catalysis, 1993. **144**: p. 93-108.
48. Rodriguez, N.M., A. Chambers, and R.T.K. Baker, *Catalytic engineering of carbon nanostructures.* Langmuir, 1995. **11**: p. 3862-3866.
49. Park, C., N.M. Rodriguez, and R.T.K. Baker, *Carbon deposition on iron-nickel during interaction with carbon monoxide-hydrogen mixtures.* Journal of Catalysis, 1997. **169**(1): p. 212-227.
50. Dry, M.E., T. Shingles, L.J. Boshoff, and C.S. van H. Botha, *Factors influencing the formation of carbon on iron Fischer-Tropsch catalysts : II. The effect of temperature and of gases and vapors present during Fischer-Tropsch synthesis.* Journal of Catalysis, 1970. **17**(3): p. 347-354.
51. Krishnankutty, N., C. Park, N.M. Rodriguez, and R.T. Baker, *The effect of copper on the structural characteristics of carbon filaments produced from iron catalyzed decomposition of ethylene.* Catalysis Today, 1997. **37**: p. 295-307.
52. Rodriguez, J.A. and G.D. Wayne, *Surface science studies of the electronic and chemical properties of bimetallic systems.* Journal of Physical Chemistry, 1991. **95**(95).
53. Huang, H., H. Kajiura, Y. Marakami, and M. Ata, *Metal sulfide catalyzed growth of carbon nanofibers and nanotubes.* Carbon, 2003. **41**: p. 615-618.
54. Tan, C.D. and R.T.K. Baker, *The effect of various sulfides on carbon deposition on nickel-iron particles.* Catalysis Today, 2000. **63**: p. 3-20.
55. Rodriguez, N.M., M.S. Kim, F. Fortin, I. Mochida, and R.T.K. Baker, *Carbon deposition on iron-nickel alloy particles.* Applied Catalysis A: General, 1997. **148**: p. 265-282.
56. Martin-Gullon, I., J. Vera, J.A. Conesa, J.L. Gonzalez, and C. Merino, *Differences between carbon nanofibers produced using Fe and Ni catalysts in a floating catalyst reactor.* Carbon, 2006. **44**: p. 1572-1580.

57. Fan, Y.-Y., H.-M. Cheng, Y.-L. Wei, G. Su, and Z.-H. Shen, *Tailoring the diameters of vapor-grown carbon nanofibers.* Carbon, 2000. **38**: p. 921-927.
58. Tibbetts, G.G., C.A. Bernardo, D.W. Gorkiewicz, and R.L. Alig, *Role of sulfur in the production of carbon fibers in the vapor phase.* Carbon, 1994. **32**: p. 569-576.
59. Sadezky, A., H. Muckenhuber, H. Grothe, R. Niessner, and U. Pöschl, *Raman microspectroscopy of soot and related carbonaceous materials: Spectral analysis and structural information.* Carbon, 2005. **43**(8): p. 1731-1742.
60. Katagiri, G., H. Ishida, and A. Ishitani, *Raman spectra of graphite edge planes.* Carbon, 1988. **26**(4): p. 565-571.
61. Jawhari, T., A. Roid, and J. Casado, *Raman spectroscopic characterization of some commercially available carbon black materials.* Carbon, 1995. **33**(11): p. 1561-1565.
62. Socrates, G., *Infrared and Raman characteristic group frequencies : tables and charts*. 3rd ed. ed, ed. G. Socrates. 2001, Chichester, West Sussex: John Wiley & Sons, Ltd.
63. Li, W.Z., X. Yan, K. Kempa, Z.F. Ren, and M. Giersig, *Structure of flattened carbon nanotubes.* Carbon, 2007. **45**: p. 2938-2945.
64. Hansen, P., *Physical Metallurgy*. 2nd ed. 1986, Cambridge, England: Cambridge University Press.
65. Matter, P.H., E. Wang, J.-M.M. Millet, and U.S. Ozkan, *Characterization of the iron phase in CN_x-based oxygen reduction reaction catalysts.* Journal of Physical Chemistry C, 2007. **111**: p. 1444-1450.
66. Biddinger, E.J., D. von Deak, and U.S. Ozkan, *Nitrogen-containing carbon nanostructures as oxygen-reduction catalysts.* Topics in Catalysis, 2009. **52**: p. 1566-1574.
67. Matter, P.H., E.J. Biddinger, and U.S. Ozkan, *Non-precious metal oxygen reduction catalysts for PEM fuel cells*, in *Catalysis*, J.J. Spivey, Editor. 2007, The Royal Society of Chemistry: Cambridge, UK. p. 338-361.
68. Garsany, Y., O.A. Baturina, and K.E. Swider-Lyons, *Impact of sulfur dioxide on the oxygen reduction reaction at Pt/Vulcan carbon electrocatalysts.* Journal of the Electrochemical Society, 2007. **154**: p. B670-B675.